Enhancement of phytoplankton biomass leeward of Tahiti as observed by Biogeochemical-Argo floats

Raphaëlle Sauzède, Elodie Martinez, Christophe Maes, Orens Pasqueron de Fommervault, Antoine Poteau, Alexandre Mignot, Hervé Claustre, Julia Uitz, Laurent Oziel, Keitapu Maamaatuaiahutapu, et al.

Enhancement of phytoplankton biomass leeward of Tahiti as observed by Biogeochemical-Argo floats

Raphaëlle Sauzède[1,2], Elodie Martinez[1,3], Christophe Maes[3], Orens Pasqueron de Fommervault[4,5], Antoine Poteau[6], Alexandre Mignot[6,7], Hervé Claustre[6], Julia Uitz[6], Laurent Oziel[6], Keitapu Maamaatuaiahutapu[2], Martine Rodier[1], Catherine Schmechtig[6] and Victoire Laurent[8]

[1]Ecosystèmes Insulaires Océaniens (EIO, UMR-241), IRD, Ifremer, UPF and ILM, Tahiti, French Polynesia
[2]Laboratoire de Géosciences du Pacifique Sud, Université de la Polynésie française, Tahiti, French Polynesia
[3]Laboratoire d'Océanographie Physique et Spatiale (LOPS), IUEM, Univ. Brest, Ifremer, CNRS, IRD, F-29280, Brest, France
[4]Departamento de Oceanografìa Fisica, Centro de Investigacion Cientìfica y de Educacion Superior de Ensenada, Carretera Ensenada-Tijuana 3918, Zona Playitas, Ensenada, BC 22860, Mexico
[5]ALSEAMAR-ALCEN company, 60 avenue Olivier Perroy, 13790 Rousset, France
[6]Sorbonne Universités, UPMC Univ Paris 06, CNRS-INSU, Observatoire Océanologique de Villefranche, Laboratoire d'Océanographie de Villefranche, 181 Chemin du Lazaret, 06230 Villefranche-Sur-Mer, France
[7]Mercator Océan, 31520 Ramonville Saint-Agne, France
[8]Direction Inter Régionale de Polynésie Française, Météo France, BP 6005 98702 Tahiti, French Polynesia

Correspondance to: Raphaëlle Sauzède (raphaelle.sauzede@gmail.com)

Keywords: Phytoplankton biomass; Biogeochemical Argo floats; Island Mass Effect; South Pacific Subtropical Gyre

Abstract. The South Pacific Subtropical Gyre (SPSG) is a vast and remote oceanic system where the variability in phytoplankton biomass and production is still largely uncertain due to the lack of *in situ* biogeochemical observations. The SPSG is an oligotrophic environment where the ecosystem is controlled predominantly by nutrient depletion in surface waters. However, this dynamic is altered in the vicinity of islands where increased biological activity occurs (i.e. the island mass effect, IME). This study mainly focuses on *in situ* observations which show evidence of an IME leeward of Tahiti (17.7°S - 149.5°W), French Polynesia. Physical and biogeochemical observations collected with two Biogeochemical-Argo profiling floats are used to investigate the dynamics of phytoplankton biomass. Data from the first float, drifting from April 2015 to November 2016 over more than 1 000 km westward of Tahiti, describe the open ocean conditions. The second float, deployed leeward of Tahiti in October 2015, stayed within 45 km off Tahiti for three months before it stopped communicating. In the oligotrophic central SPSG, our observations show that the deepening of the deep chlorophyll maximum (DCM) from winter to summer is light-driven and that the wintertime increase in chlorophyll *a* concentration in the upper layer is likely to be due to the process of photoacclimation, consistent with previous observations in oligotrophic environments. In contrast, leeward of Tahiti, the DCM widens towards the surface during late spring in association with a biological enhancement in the upper layer. Using Biogeochemical-Argo data, meteorological data from Tahiti, Hybrid Coordinate Ocean Model outputs and satellite-derived products (i.e., horizontal currents and associated fronts), the physical

mechanisms involved in producing this biological enhancement leeward of Tahiti have been investigated. The IME occurs during a period of strong precipitation and in a zone of weak currents downstream of the island. We conjecture that the land drainage induces a significant supply of nitrate in the ocean upper layer (down to ~100 m) while a zone of weak currents in the southwestern zone behind Tahiti allows an accumulation zone to form, hence increasing phytoplankton growth up to 20 km away from the coastlines. A bio-optical-based community index suggests that the composition of the phytoplankton community differs leeward of Tahiti from that in the open ocean area, with more microphytoplankton within the IME, which is associated with an increase in the carbon export to the deeper ocean.

1 Introduction

Phytoplankton is an essential component in marine biogeochemical cycles because its spatiotemporal distribution drives the trophic structure of marine ecosystems (Iverson, 1990) and constrains the variability and the production of the world ocean's fisheries (Chassot et al., 2010). Oligotrophic environments are commonly defined as regions of the global ocean where surface waters are nutrient depleted, resulting in a lack of new production (Hamner and Hauri, 1981), and where surface chlorophyll *a* concentration (Chl), a widely used proxy of phytoplankton biomass, is lower than 0.1 mg m^{-3} (Antoine et al., 1996). Although oligotrophic regions account for more than 50% of the global ocean, few studies have investigated the seasonal variability of the vertical distribution of phytoplankton biomass in these environments (Letelier et al., 2004; Mignot et al., 2014).

The South Pacific Subtropical Gyre (SPSG) is the most oligotrophic ocean area (Dandonneau et al., 2006; Morel et al., 2010) and the largest oceanic desert of the planet (Claustre and Maritorena, 2003). The SPSG is also one of the least known and least studied oceanic regions because it is vast and remote and there are few *in situ* biogeochemical observations (Sauzède et al., 2015) and large uncertainties in phytoplankton biomass variability. This gyre is also distinguished by its weak sources of nutrients from both deep layers (Raimbault et al., 2008), and the atmosphere (Claustre et al., 2008; Mahowald et al., 2005; Wagener et al., 2008). In these nutrient depleted surface waters, the biological enrichment reported near many islands, the "Island Mass Effect" (IME; Doty and Oguri, 1956), locally enhances the productivity and potential fisheries (Gove et al., 2016). By supporting a greater abundance of fish and reef-building organisms in comparison with more oligotrophic waters, the IME-induced nearshore biological enhancement is also critical for the development of coral reef ecosystems and their sustainability (Williams et al., 2015). The IME may result from the vertical transport of nutrient-rich water masses from coastal upwelling, eddy-induced mixing or internal waves (e.g. Heywood et al., 1990; Palacios, 2002; Signorini et al., 1999) or from island-related inputs such as submarine groundwater discharge or river outflow (e.g. Dandonneau and Charpy, 1985; Perissinotto et al., 2000). A recent Pacific basin-scale study showed that the IME is nearly always present in island- and atoll-reef ecosystems (Gove et al., 2016). Unfortunately, Gove et al. (2016) limited their study to 20°S - 30°N and 140°E - 150°W (mainly westward of the dateline), which exclude the eastern part of the SPSG. Moreover, most studies dealing with the phytoplankton biomass signature of the IME use satellite data (e.g. Palacios, 2002;

Martinez and Maamaatuaiahutapu, 2004; Andrade et al., 2014), and thus, miss the main part of the euphotic layer where phytoplankton photosynthesis takes place (Morel and Berthon, 1989). However, the nearshore enhancement of phytoplankton biomass occurs within the whole euphotic layer (Gove et al., 2016). Thus, in order to evaluate the impact of the IME on the vertical distribution of phytoplankton biomass it is necessary to have *in situ* measurements throughout the water column.

The incorporation of miniaturized biogeochemical sensors on autonomous profiling floats since the early 2000s offers a new and promising way of observing hydrological and key biogeochemical properties at the spatial and temporal scales needed for understanding key biogeochemical processes. Data from Biogeochemical-Argo (BGC-Argo) floats (Johnson and Claustre, 2016) have been used to investigate a variety of processes in the open ocean with unprecedented temporal and vertical resolution (e.g. Boss and Behrenfeld, 2010; Green et al., 2014; Mignot et al., 2014, 2016; Grenier et al., 2015; Sauzède et al., 2016; Zhang et al., 2016; Chacko, 2017; and references therein). More specifically for oligotrophic environments, Mignot et al. (2014, hereafter referred to as M2014) demonstrated the potential for BGC-Argo data to investigate the seasonal dynamics of the vertical distribution of phytoplankton biomass. In oligotrophic environments, M2014 showed (for four different oligotrophic environments in the global ocean) that 1) the seasonal displacement of the deep chlorophyll maximum (DCM) is light-driven, 2) the increase in Chl in the upper euphotic mixed layer always results from photoacclimation to the reduced irradiance and 3) there is an increase in phytoplankton biomass at the DCM during summer. Their study is the only investigation to date of the seasonal dynamics of the vertical distribution of phytoplankton biomass in the SPSG examining a year of measurements (over 2009) that focused on the eastern South Pacific ultra-oligotrophic environment (white star in Figure 1a). However, due to limitations in the float equipment, some fundamental variables were not measured, such as Photosynthetically Available Radiation (PAR, derived from downward irradiance measured at 490 nm) and nitrate concentration, which are primary drivers for phytoplankton growth (Cullen, 2015).

Two BGC-Argo floats were deployed leeward of the island of Tahiti (17.7° S, 149.5° W), French Polynesia, in 2015: one in April and one in October (Figure 1). They followed two distinct pathways. One float drifted during ~1.5 years in the open ocean SPSG more than 1 000 km west of Tahiti (referred to as FOpenO, Figure 1b) while the second float remained during 3 months within 45 km leeward of Tahiti (referred to as FLeeT, Figure 1c). These two floats allowed the observation of phytoplankton biomass dynamics over a broad range of scales, from seasonal in the open ocean to shorter time scales leeward of Tahiti. The present study has three main objectives: (1) to investigate the seasonal dynamics of the phytoplankton biomass in the open ocean of the SPSG; (2) to compare the FOpenO dynamics and variability with the ~3 month drift of FLeeT; (3) to identify and characterize the key mechanisms impacting the vertical distribution of phytoplankton biomass that leads to the signature of the Tahitian IME.

2 Data and Methods

2.1 Biogeochemical-Argo measurements

In this study, we use two BGC-Argo floats, FOpenO and FLeeT, also identified from their World Meteorological Organization (WMO) numbers as 6901687 and 6901659, respectively (http://www.argo.ucsd.edu, http://argo.jcommops.org). The two floats are equipped with a Seabird standard conductivity-temperature-depth (CTD) rosette with additional sensor packages. For both floats, the Satlantic OCR radiometer measures the downwelling irradiance at three wavelengths (380 nm, 410 nm and 490 nm) as well as the PAR; the WET Labs ECO Puck Triplet is composed of a chlorophyll *a* fluorometer, a Colored Dissolved Organic Matter (CDOM) fluorometer, and a sensor that measures the backscattering coefficient at 700 nm. Only FLeeT is additionally equipped with an oxygen Aanderaa optode (model 4330) that measures the oxygen concentration, and a Satlantic Submersible Ultraviolet Nitrate Analyzer (SUNA) sensor that measures the nitrate concentration. The mission parameters and equipment relative to each float used in this study are summarized in Table 1 and their respective trajectories are shown in Figure 1. A technical issue caused FLeeT to stop communicating after 3 months of drift, shortening the time series of this float.

The fluorescence of chlorophyll *a* can be considered as a proxy for chlorophyll *a* concentration (Cullen, 1982, 2015), despite the fact that the relationship between chlorophyll *a* concentration (Chl, see acronym definitions in Table 2) and fluorescence is complex, since it depends on phytoplankton community composition and physiology as well as light and nutrient availability (e.g. Cleveland and Perry, 1987; Roesler and Barnard, 2013; Sackmann et al., 2008). In this study, each profile of chlorophyll *a* fluorescence is converted into Chl using the following procedure. First, the BGC-Argo recommended protocol described by Schmechtig et al. (2014; 1, 2 and 8 quality control flags are used) is applied to each profile. The instrumental dark signal and negative spikes are removed from fluorescence profiles. The daytime non-photochemical quenching (NPQ) process that occurs at high irradiance (Cullen and Lewis, 1995) and results in a decrease of phytoplankton fluorescence per unit of Chl is corrected according to the method developed by Xing et al. (2012), using a depth threshold of 90% of the mixed layer depth (see details in Schmechtig et al., 2014). The recommended global bias correction factor of 2 is applied to each calibrated fluorescence profile (Roesler et al., 2017). Finally, profiles are also corrected from the fluorescence originating from non-algal matter as suggested by Xing et al. (2017). *In situ* Chl determinations from High Performance Liquid Chromatography (HPLC) analyses were performed during the FLeeT deployment. The Chl values derived from the fluorescence profile measured by FLeeT are correlated with those obtained from the HPLC analyses ($R^2 = 0.92$ and slope of 1.27 using a linear regression, Figure S1a), suggesting that the procedure used in calibrating the BGC-Argo fluorescence measurements is robust.

The backscattering sensors on the BGC-Argo floats measure the angular scattering coefficient at 124° relative to the direction of light propagation and at a wavelength of 700 nm. This measurement is transformed into the particulate backscattering coefficient at 700 nm, $b_{bp}(700)$ (hereafter b_{bp}), following Schmechtig et al. (2016). As in Sauzède et al. (2016), a quality control procedure is applied to each b_{bp} profile by removing: (1) high frequency spikes by using a 7-point running

median filter and (2) b_{bp} values outside of the sensor operation range (> 0.03 m^{-1}). The b_{bp} values can be interpreted in terms of Particulate Organic Carbon stock (POC; Loisel et al., 2001, 2002, Stramski et al., 1999, 2008). Stramski et al. (2008) established a relationship between POC and $b_{bp}(555)$ in the SPSG based on measurements collected during the BIOSOPE cruise (Claustre et al., 2008). Here, to estimate POC from the $b_{bp}(700)$ measurements acquired by the two BGC-Argo floats, $b_{bp}(700)$ is converted into $b_{bp}(555)$ using the commonly used power law model of the particulate backscattering spectral dependency (e.g. Loisel et al., 2006; Reynolds et al., 2001; Stramska et al., 2003):

$$b_{bp}(\lambda) = b_{bp}(\lambda_0).(\frac{\lambda}{\lambda_0})^{-\gamma} \quad (1)$$

with γ = 2.5. This value of γ is derived from *in situ* b_{bp} measurements in the SPSG, at different wavelengths from the BIOSOPE dataset (during austral summer 2004) and is in agreement with the study of Loisel et al. (2006) which found that low chlorophyll waters of subtropical gyres were associated with high γ values (between 2 and 3) because of a dominance of small-sized particles. Finally, from $b_{bp}(555)$ estimates and using the POC *vs.* $b_{bp}(555)$ slope developed from the BIOSOPE dataset excluding upwelling data (Stramski et al., 2008), b_{bp} is converted into POC for FOpenO and FLeeT.

The dissolved oxygen concentration (O_2) is derived from the Aanderaa optode measurements following the procedure described by Thierry et al. (2016). Based on the pre-deployment in-air measurements from FLeeT, a factor of 1.07 and no offset are applied to each O_2 profile (Bittig and Körtzinger, 2015).

The SUNA sensor measures the nitrate concentration (NO_3^-) from light absorption at ultraviolet wavelengths (Johnson et al., 2010, 2013; Johnson and Coletti, 2002). As recommended by Johnson et al. (2016), NO_3^- is calculated using the algorithm developed by Sakamoto et al. (2009). All data used in this study are also pressure-corrected as first suggested by Pasqueron de Fommervault et al. (2015) and confirmed by laboratory measurements (Johnson et al., 2016, 2017a, 2017b). A post-deployment calibration is finally performed to correct data from instrumental drift. Each nitrate profile is then adjusted using a reference value at depth (i.e. 900 - 950 m), estimated with an accuracy of 0.65 µmol kg^{-1} from the CANYON method (for CArbonate system and Nutrients concentration from hYdrological properties and Oxygen using a Neural network; Sauzède et al., 2017). The NO_3^- data collected by FLeeT are consistent with *in situ* NO_3^- data from the SEAL-AA3 continuous Flow Analyzer (R^2 = 0.97 and slope of 1.02 using a linear regression, Figure S1b).

The CTD data are quality controlled following the standard Argo protocol (Wong et al., 2015). The mixed layer depth (MLD) is defined as the depth at which the potential density (σ) differs from that at 10 m by 0.125 kg m^{-3} (a reference for studies regarding subtropical gyres; e.g. Levitus, 1982; Ohno et al., 2004; Suga et al., 2004; Nicholson et al., 2015; Toyoda et al., 2015).

The cell residence time in the mixed layer during a convection event is proportional to the MLD at the first order (Mignot et al., 2016, see their equation B4). In the extremely deep mixed layer (ML) in the North Atlantic (800 – 1 000 m), phytoplankton cells complete one revolution per day in the ML during convective mixing (D'Asaro, 2008). Since the MLD in the SPSG is much shallower than in the North Atlantic, we can reasonably assume that the cells make a revolution in less

than a day in the SPSG ML, suggesting that within a given day, all phytoplankton cells experience all light conditions in the ML. Consequently, as also described by Mignot et al. (2018), the average radiant energy that phytoplankton cells receive per day is obtained by averaging the vertical profile of daily PAR over the depth of the mixed layer (PAR_{ML}). Chl and b_{bp} are averaged from the surface to the first penetration depth (Z_{pd}, a reference depth for ocean color remote sensing studies) and referred as Chl_{surf} and b_{bp_surf}. Z_{pd} is here defined as $1/K_d(PAR)$ (Gordon and McCluney, 1975) with $K_d(PAR)$ being the diffuse attenuation coefficient for PAR as derived from the following equation:

$$PAR(z) = PAR(0^-)e^{-K_d(PAR)*z} \quad (2)$$

where $PAR(0^-)$ is the PAR just below the sea surface. Finally, the euphotic depth, Z_{eu}, is calculated as the depth where the PAR is reduced to 1% of its surface value.

A running average box filter is used to smooth the high frequency signals. A running average box filter of 30 days (±15 observations when data were recorded daily, until 16/07/2016, and ±3 observations when data were recorded every 5 days, after 16/07/2016) is applied to the FOpenO data to highlight the seasonal dynamics. Considering the short time of acquisition of FLeeT, the running average box filter is adjusted to 10 days (±5 observations).

2.2 HYCOM modeled ocean currents

The ocean current dataset from the daily archive of the 1/12° reanalysis of the Hybrid Coordinate Ocean Model (HYCOM, http://hycom.org; Chassignet et al., 2009) using the Navy Coupled Ocean Data Assimilation (NCODA) system is used to provide an overview of the currents in the study area and along the float trajectories. The NCODA system (Cummings, 2005; Cummings and Smedstad, 2014) assimilates available satellite altimeter observations, satellite and *in situ* Sea Surface Temperature (SST) as well as available *in situ* vertical temperature and salinity profiles (from XBTs, Argo floats and moored buoys). The GLBu0.08/expt_91.1 experiment provides ocean currents from the surface down to 300 m over the central SPSG in the area bounded by 170°W- 140°W and 10°S- 30°S from April 2015 to November 2016.

2.3 Satellite-derived products

The Chl satellite multi-mission data used in this study were obtained from the version 3 dataset of the Ocean Climate – Climate Change Initiative (OC-CCI, http://www.oceancolour.org/; Sathyendranath et al., 2018) from the European Space Agency (ESA).

To analyse fronts, transport barriers and horizontal stirring induced by surface currents, we used the Finite Size Lyapunov Exponents (FSLEs), passive Lagrangian diagnostics derived from ocean surface geostrophic currents (e.g. d'Ovidio et al., 2004; Mancho et al., 2008). FSLEs are currently provided by AVISO+ (Archiving Validation and Interpretation of Satellite Oceanographic Data, www.aviso.altimetry.fr) with a spatial resolution of 1/25° and a temporal resolution of 4 days. These data are extracted over the same region and period as described in Section 2.2 for the HYCOM dataset.

2.4 Precipitation data

The daily precipitation data are provided by the French Meteorological Institute in French Polynesia. Data were acquired from 4 meteorological stations located along the south-eastern coast of Tahiti (i.e., stations Afaahiti 3, Teahupoo 1, Teahupoo 2 and Vairao 2, locations given in Section 3.3.2).

3 Results and Discussion

3.1 Seasonal dynamics of phytoplankton biomass in the central SPSG

The seasonal dynamics of the Chl, POC and PAR vertical distributions and associated density in the open ocean are evaluated from FOpenO (Figure 2). A Deep Chlorophyll Maximum (DCM) is established throughout the FOpenO. The DCM (calculated as the depth where Chl is maximum) reaches its deepest position (~150 m) as well as the highest Chl (~0.35 mg m^{-3}) and POC values (~60 mg m^{-3}) during austral spring and summer (i.e., from September to March; Figures 2a and 2b and Table 3 for monthly average values). The DCM depth follows isolumes (red and black lines in Figure 2c). The depths of the DCM and of the specific isolume of 1 mol photons m^{-2} d^{-1} are significantly correlated (r = 0.96 and p-value < 2.2 10^{-16} using Pearson's test).

The wintertime shoaling of the DCM from April to August is associated with an increase in Chl in the 0 – 50 m upper layers and a deepening of the ML (Figures 2a and 2d and Table 3). From the surface to the first penetration depth (Z_{pd} in Figure 3a, blue line), Chl_{surf} is maximum while POC_{Surf} is low and the ratio of b_{bp_surf} and Chl_{surf}, is minimum during austral winter (blue lines, Figures 3b-e). The b_{bp} signal is dominated by sub-micronic (0.1 - 10 µm size range) particles and phytoplankton cells (Behrenfeld et al., 2005; Huot et al., 2007, 2008; Loisel et al., 2007; Morel and Ahn, 1991). It has been shown to be a good estimate of phytoplankton carbon and is used to track changes in phytoplankton biomass (Behrenfeld et al., 2005; Graff et al., 2015; Martinez-Vicente et al., 2013). Thus, b_{bp_surf}/Chl_{surf} allows the tracking of changes in phytoplankton physiology resulting from photoacclimation (Behrenfeld et al., 2005; Behrenfeld and Boss, 2003, 2006; M2014), i.e., the increase (decrease) in phytoplankton intracellular chlorophyll *a* content with the decrease (increase) in average light (Letelier et al., 1993; Morel et al., 2010; Winn et al., 1995). There is a strong relation between the seasonal variations in b_{bp_surf}/Chl_{surf} (Figure 3e) and the PAR_{ML}, the average irradiance within the ML (Figure 3f). During winter, when b_{bp_surf}/Chl_{surf} is minimum, PAR_{ML} is strongly reduced, up to a factor of about 3 with respect to summer conditions (Figure 3f). During this period, the surface irradiance intensity weakens due to strong mixing. Therefore, the observed wintertime increase in Chl_{surf} (Figure 3c) is a consequence of photoacclimation rather than an increase in phytoplankton carbon biomass. The FOpenO data shows that the wintertime Chl increase in the upper layer is due to photoacclimation and that the seasonal DCM vertical variability is light-driven in this oligotrophic SPSG environment. Thanks to direct PAR measurements, here we confirm the previously reported result in the eastern South Pacific ultra-oligotrophic environment

with PAR derived from downward irradiance measured at 490 nm (M2014).

3.2 Comparison between the central SPSG and the Tahiti nearshore environment

Surface measurements from FOpenO and in the nearshore environment downstream of Tahiti from FLeeT have been plotted together in Figure 3. During December, the mean POC_{Surf} from FLeeT is 20% higher than for FOpenO (34 mg m^{-3} *vs.* 45 mg m^{-3}; Figure 3d and Table 4). This increase in POC occurs with a slight increase in Chl_{surf} (Figure 3c), indicating an increase in phytoplankton biomass is observed leeward of Tahiti but not in the open ocean. The OC-CCI monthly composite in December 2015 (i.e., the month when the increase in POC_{Surf} and Chl $_{Surf}$ is observed from FLeeT in Figures 3c and d) shows a plume of Chl up to ~0.08 mg m^{-3} eastward of the FLeeT trajectory and near the southern coast of Tahiti (Figure 1c). This plume could be related to the biological enhancement observed in subsurface by FLeeT during December 2015 (Figures 3c and d). However, monthly composites cannot illustrate the dynamics and evolution of this event, but data coverage is too sparse at weekly scales due to cloud cover. Note that the elevated Chl values around the coastlines (up to three pixels from the coasts) are probably due to the adjacency effect that usually occurs for ocean color remote sensing in coastal waters (Bulgarelli and Zibordi, 2018).

FOpenO and FLeeT have similar light conditions (PAR_{ML}; Figure3f). Therefore, differences in b_{bp_surf}/Chl_{surf} from FOpenO and FLeeT (Figure 3e) cannot be related to photoacclimation, but probably reflect differences in phytoplankton community composition (or in the nature of the particle assemblage). Phytoplankton community composition in the SPSG is usually dominated by pico- and nano-phytoplankton (e.g. Ras et al., 2008). Cetinić et al. (2015) showed that b_{bp}/Chl can be used as a proxy for community composition with high values associated with pico- and nano- and low values associated with diatom-dominated communities. Despite the fact that the SPSG trophic conditions are very different from those investigated by Cetinić et al. (2015) in the North Atlantic Subpolar Gyre and that the b_{bp}/Chl can be affected by a change in the composition (size and nature) of the particle assemblage, the difference in average b_{bp_surf}/Chl_{surf} of a factor of 2 between FLeeT and FOpenO (Figure 3e) suggests a phytoplankton community containing a significant proportion of microphytoplankton leeward of Tahiti. Such an increase could be attributed to diatoms, which grow relatively fast and have high affinities for nitrates (Edwards et al., 2012; Glibert et al., 2016; Lomas and Glibert, 2000), and would be consistent with an increased input of nutrients leeward of Tahiti. In addition to nitrate inputs, iron inputs from land drainage could also enhance diatoms development and participate to a shift in phytoplankton community (Hendy, 2015). However, this hypothesis cannot be evaluated using BGC-Argo float observations.

To investigate if the differences in the biogeochemical dynamics between the open ocean and leeward of Tahiti observed at the surface extend to the whole water column, monthly mean vertical profiles of Chl and POC are examined from the two floats (Figure 4). The DCM depth recorded by FOpenO is at its annual deepest level during austral spring and summer (i.e. from September to March), while Chl and POC both intensify until reaching a maximum in austral summer (left panels in Figure 4), which reflects a maximum of biomass. In the FLeeT data, the DCM deepens and widens toward the

surface instead of sharpening, in association with low Chl and POC values in December and January (right panels in Figure 4). The POC vertical distribution from FOpenO shows a deep POC maximum, similar to the DCM behaviour and likely reflecting a deep biomass maximum, whereas the POC profiles from FLeeT exhibit a more homogeneous vertical distribution with a slight increase near the surface in December. Thus, the surface phytoplankton biomass enhancement leeward of Tahiti extended down to 200 m depth. In the next section, this enhancement is further investigated through the key biogeochemical parameters measured by FLeeT, such as the NO_3^- concentration.

3.3 Evidence of an island mass effect

3.3.1 Effect on phytoplankton biomass

The FLeeT data exhibit three distinct time periods as regards Chl, POC and PAR variability in the surface layer (Figures 5a and b).

The first period (from 15/10/2015 to 06/12/2015) encompasses the expected seasonal transition between the end of austral winter and the beginning of spring as observed in open ocean conditions. In October, high Chl_{surf} and low POC_{Surf} values (Figure 5a) are associated with a deep MLD (see the white line in Figures 5c-j) and low NO_3^- concentrations in the upper layer (< 1 µmol kg^{-1} in the 0 – 100 m layer, Figure 5f). These high Chl_{surf} values may be associated with photoacclimation resulting from reduced PAR_{ML} (~10 mol photons m^{-2} d^{-1}; Figure 5b). In late October, the MLD abruptly shoals and the Chl_{surf} decreases. In November the Chl_{surf} increases are associated with POC_{Surf} increases (black stars in Figure 5a), suggesting an increase in phytoplankton biomass. This point will be discussed in the next section.

The second period (from 07/12/2015 to 23/12/2015) has a simultaneous increase in Chl_{surf} and POC_{Surf} (Figure 5a), suggesting a phytoplankton biomass enhancement. During this period, there are high NO_3^- values in the upper 0 - 100 m (up to ~1.4 µmol kg^{-1}, Figures 5d and f). The NO_3^- concentrations are higher at the surface and decrease slightly under the MLD down to ~100 m (Figure 5f). When comparing POC from FOpenO and FLeeT, the POC values averaged within the Z_{pd} layer increase by a factor of ~4.5, from ~30 mg m^{-3} for FOpenO to ~140 mg m^{-3} for FLeeT (Tables 3 and 4). An increase of a factor of 1.5 is obtained when an integration is performed within the euphotic zone (~6 000 mg m^{-2} for FOpenO and ~9 000 mg m^{-2} for FLeeT, data not shown). This increase in POC in the euphotic layer (~130 m) is very clear in Figure 5i (with values larger than 60 mg m^{-3}). Below the DCM depth (red line), an increase in the frequency of POC values > 50 mg m^{-3} is indicative of more carbon export (Briggs et al., 2011, 2018) during this period. However, the export and the sinking rate cannot be quantified in this study due to the low vertical resolution of data from the FLeeT float at depth (i.e. 10 m vertical resolution, Table 1). The vertical distribution of Chl is perturbed as the DCM shoals (Figures 5c and e), and widens diapycnally (Figure 5k). In fact, the DCM seems to be associated with the 24.5 kg m^{-3} isopycnal surface over the FLeeT lifetime, except during the second time period where it is also associated with lower isopycnal surfaces (Figures 5k and 5l). Moreover, the DCM does not follow isolumes and is not light-driven as usually observed in the SPSG waters. Indeed, using

the running average box-filter (see Section 2.1) the depths of the DCM and of the isolume of 1 mol photons m^{-2} d^{-1} are not significantly correlated during this specific second period (r=0.32, p-value=0.0024 using a Pearson's test, red and black lines of period 2 in Figure 5j).

During the third period (from 24/12/2015 to 10/01/2016), the Chl_{surf}, POC_{Surf} and NO_3^- in the upper layer all decrease (Figures 5a and f). The DCM deepens from ~100 m down to ~150 m (Figure 5c), accompanied by a deepening of nitrate isocontours (Figure 5d). At the end of this period, the the conditions remind those of the SPSG open ocean.

3.3.2 Underlying physical drivers

The deviation from the classical open ocean seasonal dynamics in the FLeeT data when it reaches its closest position from Tahiti (~20 km off the coastline) suggests a potential strong influence of the island. Enhanced phytoplankton biomass can result from various processes such as uplift of nutrient-rich deep waters (e.g. coastal upwelling, eddy induced mixing; e.g. Heywood et al., 1990; Palacios, 2002; Signorini et al., 1999), terrestrial nutrient discharge due to land drainage (e.g. Dandonneau and Charpy, 1985; Perissinotto et al., 2000), or atmospheric dust deposition (e.g. Martino et al., 2014). During the second period, when the NO_3^- observed by FLeeT increases at the surface and slightly decreases under the MLD (Figure 5f), the isopycnal depths remain relatively stable (Figure 5l), suggesting that this nitrate enhancement does not result from a vertical uplift. This stability in the upper layer stratification (Figure 5l) can also be seen on the temperature profiles (Figure 5g). At larger horizontal scales, satellite sea surface temperature observations do not show any cold-water pattern leeward of Tahiti (data not shown), suggesting that there is no upwelling in the region. Moreover, there is no evidence of mesoscale eddies in satellite-derived products of sea level anomaly (data not shown). The MLD also remains shallow during this period (~40 m; Figure 5j) and does not reach the nitracline (~120 m, deduced from isoline of 1 µmol kg^{-1}; Figure 5d) so deep-water nutrients could not reach the ML. However, the increase in nitrate concentration at ~300 m (Figure 5d) when the float is the closest to Tahiti suggests that uplifting conditions could occur locally. The uplift of isotherms due to a bathymetric effect could be a factor. Coastal upwelling cannot be ruled out as a factor bringing nutrients into the area sampled by the FLeeT float. To address this question requires data from a glider equipped with a nitrate sensor that would provide biogeochemical data from the coast of Tahiti to the offshore waters. Information about island-scale internal waves (Leichter et al., 2012) would also be valuable for the investigation of the physical mechanisms involved in this IME. However, a comprehensive study of the flow field around the topographic features of the island is beyond the scope of the present analysis.

Finally, we investigate the scenario of strong precipitations over Tahiti and associated soil leaching. The runoff of sediments and other terrigenous nutrient-rich material could fertilize the offshore waters by horizontal advection. Figure 6 illustrates the FLeeT temperature/salinity (TS) diagrams from the surface down to ~200 m. A lens of low salinity water is observed very close to the surface during the second and the third periods (< 36.1 g kg^{-1}, see the black line in Figure 5h and

Figures 6a and 6b) associated with strong rain events and high NO_3^- concentrations (~1 µmol kg^{-1}) near the surface. Daily precipitation data along the south-eastern coast of Tahiti confirm that heavy rains occurred during the FLeeT drift period (Figure 7). During the first period, heavy rains were also observed, up to 300 mm at the end of November 2015, but the POC_{Surf} increase is weak with values lower than 50 mg m^{-3} (see black stars in Figure 5a) as compared with the second time period where POC_{Surf} reaches up to 140 mg m^{-3}. No NO_3^- enrichment in the upper layer is observed during the first period (Figure 5f), probably because the float is further from Tahiti (Figure 7a) or due to the consumption of nutrients by biota. During the second period, moderate precipitation, up to 120 mm, occurs while FLeeT reaches its closest position to Tahiti, about 20 km (Figure 7a). The surface nitrate concentration and salinity measurements are significantly correlated throughout the entire float lifetime (using a Pearson's test), and more correlated during period 2 ($r = -0.73$ and p-value $< 2.2\ 10^{-16}$ for the entire FLeeT lifetime; $r = -0.9$ and p-value $< 2.2\ 10^{-16}$ for the first period, $r = -0.99$ and p-value $< 2.2\ 10^{-16}$ for the second period and $r = -0.65$ and p-value $< 2.2\ 10^{-16}$ for the third period; time series of salinity and nitrate concentrations are presented in Figure S2). During period 2, land drainage likely supplied nitrate to the upper layer. The HYCOM model reanalysis shows currents along the FLeeT track with speeds between 10 cm s^{-1} and 60 cm s^{-1} during the first and third periods (Figure 8a). During the second period, the float crossed a zone of weak current with speeds lower than 10 cm s^{-1}. These currents are part of the SEC which mainly flows south-westward in the upper layers, from Tahiti toward the open ocean (Figures 8b and 8c). The float remained leeward of Tahiti in this weak current area where nitrate issued from land drainage may have accumulated. To test the hypothesis of land drainage, we performed a Lagrangian analysis following the approach discussed by *d'Ovidio et al.* (2010) and using the HYCOM surface currents. 50 fictive particles, distributed around the float position during the period 2 (i.e. circular patch centered around -149.3°E -17.92°N on 13/12/2015), were advected backward in time. The tracking of their trajectories (see Figure S3 in the supplementary material) evidenced that 100% of the virtual particles were originated from the island coasts. 18% of the particles drifted during more than 14 days and were originated from the southwestern part of the island, whereas 82% of the virtual particles were originated from the southeastern part, between the Teputa and Havae passes (Figure 7a), and drifted during less than 5 days to reach the area characterized by the increase in phytoplankton biomass.The broad vertical extension down to ~100 m of the nitrate enhancement (~1.4 µmol kg^{-1}, Figure 5f) could be explained by the intense (horizontal and/or vertical) currents flushing out of the passes of the lagoon could advect nutrient-enhanced waters toward the open ocean. In Moorea (the closest island westward of Tahiti, Figure 1c), the current flushing out of the pass has an average of 50 cm s^{-1} and can even reach 200 cm s^{-1} (Lenhardt, 1991). These currents cannot be described by the present ocean reanalysis HYCOM since it does not take into account the specific lagoon dynamics and exchanges with open ocean waters.

During the third period, relatively strong precipitation occurs in Tahiti without an increase in phytoplankton (Figure 5a) as the float drifts away from the island. There is a clear change in the ocean dynamics between the second and the third period. The float flows south-westward within a strong branch of the SEC with speeds higher than 30 cm s^{-1} down to 300 m

and up to 60 cm s^{-1} in its core (Figure 8a). During period 2, the TS diagram shows a classical structure highlighting two water masses in the upper 300 m with the SubTropical Surface Water (STSW: S > 36 g kg^{-1}) at the top and the Eastern South Pacific Central Waters (ESPCW : temperature between 8 and 24°C and salinity between 34.4 and 36.4 g kg^{-1}) at the bottom. Over period 3, the thermocline waters are more mixed and the signature of the third water mass located between the isopycnal surfaces 24.5 and 25 kg m^{-3} is dampened (Figure 6b). At these depths (i.e., below 150 m) changes can also be observed from period 2 to 3 on the oxygen vertical distribution (Figure 9). Indeed, during the third period FLeeT drifts across a more oxygenated water mass in the 150 - 350 m layer that likely comes from the south. HYCOM shows a south-westward-flowing subsurface current at 300 m close to Tahiti during the transition between the second and the third periods (Figure 8). However, it is necessary to take into account the time lag to allow the water mass to reach Tahiti before the transition period. Indeed, when considering position A, south of Tahiti (Figure 10), the time to reach position B is about 24 days. More oxygenated waters were observed by FLeeT on 28/12/2015 and the HYCOM currents on 04/12/2015 suggest that the oxygenated water mass has its origin in the south. We also investigated satellite derived FSLEs, which provide information about fronts, transport barriers and horizontal stirring by surface currents. Figures 11a and 11b show that the float crosses a front coming from the east during the transition period (dark grey filament east and along the crosses, respectively). These figures illustrate the rapid and intense evolution of the water mass, evidenced from O_2 and TS diagrams, and the fact that the float quickly leaves the area of nutrient accumulation to come back to a nutrient-depleted environment (Figures 5b, c and f), typical of the SPSG oligotrophic conditions. It is difficult to interpret observations of a different nature, i.e., from a Lagrangian *vs*. Eulerian point of view. Meso to submeso-scale dynamics and fronts represent barriers to transport, and further work is required to place the float observations in the full dynamical context of the flow at these different scales, following methods developed by Mendoza and Mancho (2010) for instance. Moreover, because of the Lagrangian nature of profiling floats data, it is not possible to determine whether the biological enhancement observed in FLeeT corresponds to the horizontal extent of the IME or if it is more a temporary signal. Further observations such as glider data are required to fully describe this IME.

5 Summary and conclusion

Two Biogeochemical-Argo (BGC-Argo) profiling floats deployed in the central subtropical gyre of the Pacific Ocean provided an unprecedented source of information in this scarcely sampled remote area. These observations were used to describe the seasonal dynamics of phytoplankton biomass in the SPSG open ocean. In the open waters southwest off Tahiti, the FOpenO observations showed that the wintertime chlorophyll *a* concentration (Chl) increase in the upper layer is likely due to photoacclimation and that the seasonal deep chlorophyll maximum (DCM) vertical variability is light-driven in the open ocean oligotrophic South Pacific Subtropical Gyre (SPSG). The float near the coast of Tahiti allowed us to investigate the dynamics of phytoplankton biomass leeward of Tahiti and to compare it with open ocean conditions. The phytoplankton dynamics were different near the island over several weeks in late austral spring 2015, with an increase in Chl, particulate

organic carbon (POC) and nitrate (NO_3^-) concentrations within the 100 m upper layer, and a shallowing and widening of the DCM. During this period the vertical position of the DCM was no longer light-driven. The particulate backscattering coefficient (b_{bp}) measurements below the DCM depth suggest an increase in the carbon export during the biological enhancement and the b_{bp}/Chl optics-based index suggest a shift in phytoplankton community composition from a pico- and nano-dominated community in the open ocean toward a micro-dominated community leeward of Tahiti. The b_{bp}/Chl index could also suggest changes in the composition (size and nature) of the particle assemblage rather than in the phytoplankton community structure only.

Combining BGC-Argo float data, meteorological data, ocean modeling and satellite data, the physical mechanisms involved in the phytoplankton increase leeward of Tahiti have been investigated. Land drainage induced by strong precipitation on Tahiti and weak south-westward currents could have supplied nutrients leeward of Tahiti to support the enhanced productivity observed in FLeeT data. Since HYCOM does not take into account the specific lagoon dynamics, a more dedicated project incorporating lagoon modeling is needed to understand nutrient inputs. Profiling floats are Lagrangian platforms that do not allow us to determine if the observed biological enhancement is associated with a temporal event or if it represents the horizontal extent of the island mass effect (IME). Further hydrological and biogeochemical measurements from the Tahiti coast to offshore waters collected by gliders or ocean modeling combined with Lagrangian particle tracking are necessary to resolve this issue.

For the first time the vertical signature of an IME has been studied from BGC-Argo float observations. This IME could not have been observed by ocean color satellite data because of the high cloud coverage in this region. The FLeeT measurements provide the first description of an IME around Tahiti, showing a surface biological enhancement up to 20 km off Tahiti, which was probably driven by land drainage induced by strong precipitation on Tahiti. BGC-Argo floats provide valuable data on the distribution of subsurface Chl and other biogeochemical and bio-optical parameters that are not available by remote sensing. Mechanisms involved in the IME are complex and vary from one island to another, but by combining BGC-Argo float, meteorological data, ocean modelling and satellite data, we hypothesize that the IME downstream of the island of Tahiti is the result of nutrient influx caused by land drainage following precipitations events. However, additional uplift of nutrient-rich deep waters through coastal upwelling cannot be totally excluded from our results.

The present study demonstrates that nearshore phytoplankton enhancement can be significant and can impact the vertical distribution of phytoplankton biomass. It also probably impacts its community composition and the associated carbon export. In oligotrophic environments, where ecosystems are predominantly characterized by nutrient-depleted waters, the increase in phytoplankton biomass driven by the IME is critical for coral reef ecosystems (Williams et al., 2015) and fishery productivity but also contributes to carbon vertical flow (Heywood et al., 1996). Such biological enhancement needs to be carefully described and studied in order to be integrated into global biogeochemical models, and hopefully to better predict the evolution of nearshore marine ecosystems.

In the SPSG, climate change is likely to impact open ocean food webs and oceanic fisheries (Bell et al., 2011). It is therefore important to document changes in biogeochemical processes using long observational time series. BGC-Argo profiling floats are powerful tools to track ecological and biogeochemical changes, especially in areas under-sampled by classical ship-based oceanographic cruises such as the SPSG.

Acknowledgements

We would like to thank the Government of French Polynesia and the French State for providing funding support to the THOT project (Contrat de projets Etat-Pays, convention n°8690/MSR/REC, and arrêté de subvention n° HC/2860/DIE/BPT), including the postdoctoral fellowship of R. Sauzède. This work was also supported by the French national program LEFE/INSU and the French Ministry of the Overseas territories. FOpenO was provided by the remOcean project (funded by the European Research Council, grant agreement 246777). We also thank the French BGC-Argo program (funded by CNES-TOSCA, LEFE Cyber and LEFE-GMMC) and the Coriolis program for providing standard Argo floats to be equipped with additional bio-optical and biogeochemical sensors. The BGC-Argo data were collected and made freely available by the International Argo Program and the national programs that contribute to it. (http://www.argo.ucsd.edu, http://argo.jcommops.org/). This Argo Program is part of the Global Ocean Observing System. We would also like to thank Henry Bittig for his expertise in the calibration (slope and offset determination) of FLeeT O_2 profiles. AVISO+ (Archiving Validation and Interpretation of Satellite Oceanographic Data, www.aviso.altimetry.fr) freely provided the Finite Size Lyapunov Exponent data used in this study. The 1/12° global HYCOM+NCODA Ocean Reanalysis was funded by the U.S. Navy and the Modeling and Simulation Coordination Office. Computer time was made available by the DoD High Performance Computing Modernization Program. The output is publicly available at http://hycom.org. Data from the BIOSOPE transect of particulate backscattering coefficient at different wavelengths were taken from the BIOSOPE database available on the website: http://www.obs-vlfr.fr/proof/php/x_datalist.php?xxop=biosope&xxcamp=biosope; and access has been provided by C. Schmechtig. We would like to warmly thank Hilary Todd for the correction of the English of the manuscript. Finally, we are grateful to the anonymous Reviewers for their valuable comments and suggestions.

References

Andrade, I., Sangrà, P., Hormazabal, S. and Correa-Ramirez, M.: Island mass effect in the Juan Fernández Archipelago (33°S), Southeastern Pacific, Deep Sea Res. Part I Oceanogr. Res. Pap., 84, 86–99, doi:10.1016/j.dsr.2013.10.009, 2014.

Antoine, D., André, J.-M. and Morel, A.: Oceanic primary production: 2. Estimation at global scale from satellite (Coastal Zone Color Scanner) chlorophyll, Global Biogeochem. Cycles, 10(1), 57–69, doi:10.1029/95GB02832, 1996.

Behrenfeld, M. J. and Boss, E.: The beam attenuation to chlorophyll ratio: An optical index of phytoplankton physiology in the surface ocean?, Deep. Res. Part I Oceanogr. Res. Pap., 50(12), 1537–1549, doi:10.1016/j.dsr.2003.09.002, 2003.

Behrenfeld, M. J. and Boss, E.: Beam attenuation and chlorophyll concentration as alternative optical indices of phytoplankton biomass, J. Mar. Res., 64(3), 431–451, doi:10.1357/002224006778189563, 2006.

Behrenfeld, M. J., Boss, E., Siegel, D. A. and Shea, D. M.: Carbon-based ocean productivity and phytoplankton physiology from space, Global Biogeochem. Cycles, 19(1), GB1006, doi:10.1029/2004GB002299, 2005.

Bell, J., Johnson, J. and Hobday, A.: Vulnerability of tropical Pacific fisheries and aquaculture to climate change, Secretariat of the Pacific Community, Auckland, NZ., 2011.

Bittig, H. C. and Körtzinger, A.: Tackling Oxygen Optode Drift: Near-Surface and In-Air Oxygen Optode Measurements on a Float Provide an Accurate in Situ Reference, J. Atmos. Ocean. Technol., 32, 1536–1543, doi:10.1175/JTECH-D-14-00162.1, 2015.

Boss, E. and Behrenfeld, M.: In situ evaluation of the initiation of the North Atlantic phytoplankton bloom, Geophys. Res. Lett., 37(18), L18603, doi:10.1029/2010GL044174, 2010.

Briggs, N., Perry, M. J., Cetinić, I., Lee, C., D'Asaro, E., Gray, A. M. and Rehm, E.: High-resolution observations of aggregate flux during a sub-polar North Atlantic spring bloom, Deep Sea Res. Part I Oceanogr. Res. Pap., 58(10), 1031–1039, doi:10.1016/j.dsr.2011.07.007, 2011.

Briggs, N., Guðmundsson, K., Cetinić, I., D'Asaro, E., Rehm, E., Lee, C. and Perry, M. J.: A multi-method autonomous assessment of primary productivity and export efficiency in the springtime North Atlantic, Biogeosciences, 15(14), 4515–4532, doi:10.5194/bg-15-4515-2018, 2018.

Bulgarelli, B. and Zibordi, G.: On the detectability of adjacency effects in ocean color remote sensing of mid-latitude coastal environments by SeaWiFS, MODIS-A, MERIS, OLCI, OLI and MSI, Remote Sens. Environ., 209, 423–438, doi:10.1016/J.RSE.2017.12.021, 2018.

Cetinić, I., Perry, M. J., D'Asaro, E., Briggs, N., Poulton, N., Sieracki, M. E. and Lee, C. M.: A simple optical index shows spatial and temporal heterogeneity in phytoplankton community composition during the 2008 North Atlantic Bloom Experiment, Biogeosciences, 12(7), 2179–2194, doi:10.5194/bg-12-2179-2015, 2015.

Chacko, N.: Chlorophyll bloom in response to tropical cyclone Hudhud in the Bay of Bengal: Bio-Argo subsurface observations, Deep Sea Res. Part I Oceanogr. Res. Pap., 124, 66–72, doi:10.1016/j.dsr.2017.04.010, 2017.

Chassignet, E., Hurlburt, H., Metzger, E. J., Smedstad, O., Cummings, J., Halliwell, G., Bleck, R., Baraille, R., Wallcraft, A., Lozano, C., Tolman, H., Srinivasan, A., Hankin, S., Cornillon, P., Weisberg, R., Barth, A., He, R., Werner, F. and Wilkin, J.: US GODAE: Global Ocean Prediction with the HYbrid Coordinate Ocean Model (HYCOM), Oceanography, doi:10.5670/oceanog.2009.39, 2009.

Chassot, E., Bonhommeau, S., Dulvy, N. K., Mélin, F., Watson, R., Gascuel, D. and Le Pape, O.: Global marine primary production constrains fisheries catches, Ecol. Lett., 13(4), 495–505, doi:10.1111/j.1461-0248.2010.01443.x, 2010.

Claustre, H. and Maritorena, S.: The Many Shades of Ocean Blue, Science, 302(5650), 1514–1515, doi:10.1126/science.1092704, 2003.

Claustre, H., Sciandra, A. and Vaulot, D.: Introduction to the special section bio-optical and biogeochemical conditions in the South East Pacific in late 2004: the BIOSOPE program, Biogeosciences, 5(3), 679–691, doi:10.5194/bg-5-679-2008, 2008.

Cleveland, J. S. and Perry, M. J.: Quantum yield, relative specific absorption and fluorescence in nitrogen-limited Chaetoceros gracilis, Mar. Biol., 94(4), 489–497, doi:10.1007/BF00431395, 1987.

Cullen, J. J.: The Deep Chlorophyll Maximum: Comparing Vertical Profiles of Chlorophyll a, Can. J. Fish. Aquat. Sci., 39(5), 791–803, doi:10.1139/f82-108, 1982.

Cullen, J. J.: Subsurface chlorophyll maximum layers: enduring enigma or mystery solved?, Ann. Rev. Mar. Sci., 7, 207–39, doi:10.1146/annurev-marine-010213-135111, 2015.

Cullen, J. J. and Lewis, M. R.: Biological processes and optical measurements near the sea surface: Some issues relevant to remote sensing, J. Geophys. Res., 100(C7), 13255, doi:10.1029/95JC00454, 1995.

Cummings, J. A.: Operational multivariate ocean data assimilation, Q. J. R. Meteorol. Soc., 131(613), 3583–3604, doi:10.1256/qj.05.105, 2005.

Cummings, J. A. and Smedstad, O. M.: Ocean data impacts in global HYCOM, J. Atmos. Ocean. Technol., 31, 1771–1791, doi:10.1175/JTECH-D-14-00011.1, 2014.

D'Asaro, E. A.: Convection and the seeding of the North Atlantic bloom, J. Mar. Syst., 69(3), 233–237, doi:10.1016/j.jmarsys.2005.08.005, 2008.

d'Ovidio, F., Fernández, V., Hernández-García, E. and López, C.: Mixing structures in the Mediterranean Sea from finite-size Lyapunov exponents, Geophys. Res. Lett., 31(17), L17203, doi:10.1029/2004GL020328, 2004.

d'Ovidio, F., De Monte, S., Alvain, S., Dandonneau, Y. and Lévy, M.: Fluid dynamical niches of phytoplankton types., Pro Natl. Acad. Sci. U. S. A., 107(43), 18366–70, doi:10.1073/pnas.1004620107, 2010.
Dandonneau, Y. and Charpy, L.: An empirical approach to the island mass effect in the south tropical Pacific based on sea surface chlorophyll concentrations, Deep Sea Res. Part A. Oceanogr. Res. Pap., 32(6), 707–721, doi:10.1016/0198-0149(85)90074-3, 1985.

Dandonneau, Y., Montel, Y., Blanchot, J., Giraudeau, J. and Neveux, J.: Temporal variability in phytoplankton pigments, picoplankton and coccolithophores along a transect through the North Atlantic and tropical southwestern Pacific, Deep Sea Res. Part I Oceanogr. Res. Pap., 53(4), 689–712, doi:10.1016/j.dsr.2006.01.002, 2006.

Doty, M. S. and Oguri, M.: The Island Mass Effect, ICES J. Mar. Sci., 22(1), 33–37, doi:10.1093/icesjms/22.1.33, 1956.

Edwards, K. F., Thomas, M. K., Klausmeier, C. A. and Litchman, E.: Allometric scaling and taxonomic variation in nutrient utilization traits and maximum growth rate of phytoplankton, Limnol. Oceanogr., 57(2), 554–566, doi:10.4319/lo.2012.57.2.0554, 2012.

Glibert, P. M., Wilkerson, F. P., Dugdale, R. C., Raven, J. A., Dupont, C. L., Leavitt, P. R., Parker, A. E., Burkholder, J. M. and Kana, T. M.: Pluses and minuses of ammonium and nitrate uptake and assimilation by phytoplankton and implications for productivity and community composition, with emphasis on nitrogen-enriched conditions, Limnol. Oceanogr., 61(1), 165–197, doi:10.1002/lno.10203, 2016.

Gordon, H. R. and McCluney, W. R.: Estimation of the depth of sunlight penetration in the sea for remote sensing., Appl. Opt., 14(2), 413–6, doi:10.1364/AO.14.000413, 1975.

Gove, J. M., McManus, M. A., Neuheimer, A. B., Polovina, J. J., Drazen, J. C., Smith, C. R., Merrifield, M. A., Friedlander, A. M., Ehses, J. S., Young, C. W., Dillon, A. K. and Williams, G. J.: Near-island biological hotspots in barren ocean basins., Nat. Commun., 7, 10581, doi:10.1038/ncomms10581, 2016.

Graff, J. R., Westberry, T. K., Milligan, A. J., Brown, M. B., Dall'Olmo, G., Dongen-Vogels, V. van, Reifel, K. M. and Behrenfeld, M. J.: Analytical phytoplankton carbon measurements spanning diverse ecosystems, Deep Sea Res. Part I Oceanogr. Res. Pap., 102, 16–25, doi:10.1016/j.dsr.2015.04.006, 2015.

Green, R. E., Bower, A. S. and Lugo-Fernández, A.: First Autonomous Bio-Optical Profiling Float in the Gulf of Mexico Reveals Dynamic Biogeochemistry in Deep Waters, edited by W.-C. Chin, PLoS One, 9(7), e101658, doi:10.1371/journal.pone.0101658, 2014.

Grenier, M., Della Penna, A. and Trull, T. W.: Autonomous profiling float observations of the high-biomass plume downstream of the Kerguelen Plateau in the Southern Ocean, Biogeosciences, 12(9), 2707–2735, doi:10.5194/bg-12-2707-2015, 2015.

Hamner, W. M. and Hauri, I. R.: Effects of island mass: Water flow and plankton pattern around a reef in the Great Barrier Reef lagoon, Australia1, Limnol. Oceanogr., 26(6), 1084–1102, doi:10.4319/lo.1981.26.6.1084, 1981.

Hendy, I. L.: Ironing out carbon export to the deep ocean, Proc. Natl. Acad. Sci., 112(2), 306–307, doi:10.1073/PNAS.1421561112, 2015.

Heywood, K. J., Barton, E. D. and Simpson, J. H.: The effects of flow disturbance by an oceanic island, J. Mar. Res., 48(1), 55–73, doi:10.1357/002224090784984623, 1990.

Heywood, K. J., Stevens, D. P. and Grant, R. B.: Eddy formation behind the tropical island of Aldabra, Deep Sea Res. Part I Oceanogr. Res. Pap., 43(4), 555–578, doi:10.1016/0967-0637(96)00097-0, 1996.

Huot, Y., Babin, M., Bruyant, F., Grob, C., Twardowski, M. S. and Claustre, H.: Relationship between photosynthetic parameters and different proxies of phytoplankton biomass in the subtropical ocean, Biogeosciences, 4(5), 853–868, doi:10.5194/bg-4-853-2007, 2007.

Huot, Y., Morel, A., Twardowski, M. S., Stramski, D. and Reynolds, R. A.: Particle optical backscattering along a chlorophyll gradient in the upper layer of the eastern South Pacific Ocean, Biogeosciences, 5(2), 495–507, doi:10.5194/bg-5-495-2008, 2008.

Iverson, R. L.: Control of marine fish production, Limnol. Oceanogr., 35(7), 1593–1604, doi:10.4319/lo.1990.35.7.1593, 1990.

Johnson, K., Pasqueron De Fommervault, O., Serra, R., D'Ortenzio, F., Schmechtig, C., Claustre, H. and Poteau, A.: Processing Bio-Argo nitrate concentration at the DAC Level, Argo data management., 2016.

Johnson, K. S. and Claustre, H.: Bringing biogeochemistry into the Argo age, Eos, Trans. Am. Geophys. Union, 97, doi:10.1029/2016EO062427, 2016.

Johnson, K. S. and Coletti, L. J.: In situ ultraviolet spectrophotometry for high resolution and long-term monitoring of nitrate, bromide and bisulfide in the ocean, Deep Sea Res. Part I Oceanogr. Res. Pap., 49(7), 1291–1305, doi:10.1016/S0967-0637(02)00020-1, 2002.

Johnson, K. S., Riser, S. C. and Karl, D. M.: Nitrate supply from deep to near-surface waters of the North Pacific subtropical gyre., Nature, 465(7301), 1062–5, doi:10.1038/nature09170, 2010.

Johnson, K. S., Coletti, L. J., Jannasch, H. W., Sakamoto, C. M., Swift, D. D. and Riser, S. C.: Long-Term Nitrate Measurements in the Ocean Using the in situ Ultraviolet Spectrophotometer: Sensor Integration into the APEX Profiling

Float, J. Atmos. Ocean. Technol., 30(8), 1854–1866, doi:10.1175/JTECH-D-12-00221.1, 2013.

Johnson, K. S., Plant, J. N., Dunne, J. P., Talley, L. D. and Sarmiento, J. L.: Annual nitrate drawdown observed by SOCCOM profiling floats and the relationship to annual net community production, J. Geophys. Res. Ocean., 122(8), 6668–6683, doi:10.1002/2017JC012839, 2017a.

Johnson, K. S., Plant, J. N., Coletti, L. J., Jannasch, H. W., Sakamoto, C. M., Riser, S. C., Swift, D. D., Williams, N. L., Boss, E., Haëntjens, N., Talley, L. D. and Sarmiento, J. L.: Biogeochemical sensor performance in the SOCCOM profiling float array, J. Geophys. Res. Ocean., 122(6416–6436), doi:10.1002/2017JC012838, 2017b.

Leichter, J. J., Stokes, M. D., Hench, J. L., Witting, J. and Washburn, L.: The island-scale internal wave climate of Moorea, French Polynesia, J. Geophys. Res. Ocean., 117(C6), n/a-n/a, doi:10.1029/2012JC007949, 2012.

Lenhardt, X.: Hydrodynamique des lagons d'atoll et d'île haute en Polynésie française, Ed. de l'ORSTOM-Institut français de recherche scientifique pour le développement en coopération. [online] Available from: http://www.documentation.ird.fr/hor/fdi:34233, 1991.

Letelier, R. M., Bidigare, R. R., Hebel, D. V., Ondrusek, M., Winn, C. D. and Karl, D. M.: Temporal variability of phytoplankton community structure based on pigment analysis, Limnol. Oceanogr., 38(7), 1420–1437, doi:10.4319/lo.1993.38.7.1420, 1993.

Letelier, R. M., Karl, D. M., Abbott, M. R. and Bidigare, R. R.: Light driven seasonal patterns of chlorophyll and nitrate in the lower euphotic zone of the North Pacific Subtropical Gyre, Limnol. Oceanogr., 49(2), 508–519, doi:10.4319/lo.2004.49.2.0508, 2004.

Levitus, S.: Climatological atlas of the world ocean, NOAA Prof. Pap., 13, 1982.

Loisel, H., Bosc, E., Stramski, D., Oubelkheir, K. and Deschamps, P.-Y.: Seasonal variability of the backscattering coefficient in the Mediterranean Sea based on satellite SeaWiFS imagery, Geophys. Res. Lett., 28(22), 4203–4206, doi:10.1029/2001GL013863, 2001.

Loisel, H., Nicolas, J.-M., Deschamps, P.-Y. and Frouin, R.: Seasonal and inter-annual variability of particulate organic matter in the global ocean, Geophys. Res. Lett., 29(24), 2196, doi:10.1029/2002GL015948, 2002.

Loisel, H., Nicolas, J.-M., Sciandra, A., Stramski, D. and Poteau, A.: Spectral dependency of optical backscattering by marine particles from satellite remote sensing of the global ocean, J. Geophys. Res., 111(C9), C09024, doi:10.1029/2005JC003367, 2006.

Loisel, H., Mériaux, X., Berthon, J.-F. and Poteau, A.: Investigation of the optical backscattering to scattering ratio of marine particles in relation to their biogeochemical composition in the eastern English Channel and southern North Sea, Limnol. Oceanogr., 52(2), 739–752, doi:10.4319/lo.2007.52.2.0739, 2007.
Lomas, M. W. and Glibert, P. M.: Comparisons of nitrate uptake, storage, and reduction in marine diatoms and flagellates, J. Phycol., 36(5), 903–913, doi:10.1046/j.1529-8817.2000.99029.x, 2000.

Mahowald, N. M., Baker, A. R., Bergametti, G., Brooks, N., Duce, R. A., Jickells, T. D., Kubilay, N., Prospero, J. M. and Tegen, I.: Atmospheric global dust cycle and iron inputs to the ocean, Global Biogeochem. Cycles, 19(4), GB4025, doi:10.1029/2004GB002402, 2005.

Mancho, A. M., Hernández-García, E., Small, D., Wiggins, S., Fernández, V., Mancho, A. M., Hernández-García, E., Small, D., Wiggins, S. and Fernández, V.: Lagrangian Transport through an Ocean Front in the Northwestern Mediterranean Sea, J. Phys. Oceanogr., 38(6), 1222–1237, doi:10.1175/2007JPO3677.1, 2008.

Martinez-Vicente, V., Dall'Olmo, G., Tarran, G., Boss, E. and Sathyendranath, S.: Optical backscattering is correlated with phytoplankton carbon across the Atlantic Ocean, Geophys. Res. Lett., 40(6), 1154–1158, doi:10.1002/grl.50252, 2013.

Martinez, E. and Maamaatuaiahutapu, K.: Island mass effect in the Marquesas Islands: Time variation, Geophys. Res. Lett., 31(18), L18307, doi:10.1029/2004GL020682, 2004.

Martino, M., Hamilton, D., Baker, A. R., Jickells, T. D., Bromley, T., Nojiri, Y., Quack, B. and Boyd, P. W.: Western Pacific atmospheric nutrient deposition fluxes, their impact on surface ocean productivity, Global Biogeochem. Cycles, 28(7), 712–728, doi:10.1002/2013GB004794, 2014.

Mendoza, C. and Mancho, A. M.: Hidden Geometry of Ocean Flows, Phys. Rev. Lett., 105(3), 38501, doi:10.1103/PhysRevLett.105.038501, 2010.

Mignot, A., Claustre, H., Uitz, J., Poteau, A., D'Ortenzio, F. and Xing, X.: Understanding the seasonal dynamics of phytoplankton biomass and the deep chlorophyll maximum in oligotrophic environments: A Bio-Argo float investigation, Global Biogeochem. Cycles, 28(8), 856–876, doi:10.1002/2013GB004781, 2014.

Mignot, A., Ferrari, R. and Mork, K. A.: Spring bloom onset in the Nordic Seas, Biogeosciences, 13(11), 3485–3502, doi:10.5194/bg-13-3485-2016, 2016.

Mignot, A., Ferrari, R. and Claustre, H.: Floats with bio-optical sensors reveal what processes trigger the North Atlantic bloom, Nat. Commun., 9(1), 190, doi:10.1038/s41467-017-02143-6, 2018.

Morel, A. and Ahn, Y.-H.: Optics of heterotrophic nanoflagellates and ciliates: A tentative assessment of their scattering role in oceanic waters compared to those of bacterial and algal cells, J. Mar. Res., 49(1), 177–202, doi:10.1357/002224091784968639, 1991.
Morel, A. and Berthon, J.-F.: Surface pigments, algal biomass profiles, and potential production of the euphotic layer: Relationships reinvestigated in view of remote-sensing applications, Limnol. Oceanogr., 34(8), 1545–1562, doi:10.4319/lo.1989.34.8.1545, 1989.

Morel, A., Claustre, H. and Gentili, B.: The most oligotrophic subtropical zones of the global ocean: similarities and differences in terms of chlorophyll and yellow substance, Biogeosciences, 7(10), 3139–3151, doi:10.5194/bg-7-3139-2010, 2010.

Nicholson, D. P., Wilson, S. T., Doney, S. C. and Karl, D. M.: Quantifying subtropical North Pacific gyre mixed layer primary productivity from Seaglider observations of diel oxygen cycles, Geophys. Res. Lett., 42(10), 4032–4039, doi:10.1002/2015GL063065, 2015.

Ohno, Y., Kobayashi, T., Iwasaka, N. and Suga, T.: The mixed layer depth in the North Pacific as detected by the Argo floats, Geophys. Res. Lett., 31(11), L11306, doi:10.1029/2004GL019576, 2004.

Palacios, D. M.: Factors influencing the island-mass effect of the Galápagos Archipelago, Geophys. Res. Lett., 29(23), 49-1-49–4, doi:10.1029/2002GL016232, 2002.

Pasqueron de Fommervault, O., D'Ortenzio, F., Mangin, A., Serra, R., Migon, C., Claustre, H., Lavigne, H., Ribera d'Alcalà, M., Prieur, L., Taillandier, V., Schmechtig, C., Poteau, A., Leymarie, E., Dufour, A., Besson, F. and Obolensky, G.: Seasonal variability of nutrient concentrations in the Mediterranean Sea: Contribution of Bio-Argo floats, J. Geophys. Res. Ocean., 120(12), 8528–8550, doi:10.1002/2015JC011103, 2015.

Perissinotto, R., ELutjeharms, J. R. . and van Ballegooyen, R. .: Biological–physical interactions and pelagic productivity at the Prince Edward Islands, Southern Ocean, J. Mar. Syst., 24(3–4), 327–341, doi:10.1016/S0924-7963(99)00093-7, 2000.

Raimbault, P., Garcia, N. and Cerutti, F.: Distribution of inorganic and organic nutrients in the South Pacific Ocean − evidence for long-term accumulation of organic matter in nitrogen-depleted waters, Biogeosciences, 5(2), 281–298, doi:10.5194/bg-5-281-2008, 2008.

Ras, J., Claustre, H. and Uitz, J.: Spatial variability of phytoplankton pigment distributions in the Subtropical South Pacific Ocean: comparison between in situ and predicted data, Biogeosciences, 5(2), 353–369, doi:10.5194/bg-5-353-2008, 2008.

Reynolds, R. A., Stramski, D. and Mitchell, B. G.: A chlorophyll-dependent semianalytical reflectance model derived from field measurements of absorption and backscattering coefficients within the Southern Ocean, J. Geophys. Res. Ocean., 106(C4), 7125–7138, doi:10.1029/1999JC000311, 2001.

Roesler, C., Uitz, J., Claustre, H., Boss, E., Xing, X., Organelli, E., Briggs, N., Bricaud, A., Schmechtig, C., Poteau, A., D'Ortenzio, F., Ras, J., Drapeau, S., Haëntjens, N. and Barbieux, M.: Recommendations for obtaining unbiased chlorophyll estimates from in situ chlorophyll fluorometers: A global analysis of WET Labs ECO sensors, Limnol. Oceanogr. Methods, 15(6), 572–585, doi:10.1002/lom3.10185, 2017.

Roesler, C. S. and Barnard, A. H.: Optical proxy for phytoplankton biomass in the absence of photophysiology: Rethinking the absorption line height, Methods Oceanogr., 7, 79–94, doi:10.1016/j.mio.2013.12.003, 2013.

Sackmann, B. S., Perry, M. J. and Eriksen, C. C.: Seaglider observations of variability in daytime fluorescence quenching of chlorophyll-<i>a</i> in Northeastern Pacific coastal waters, Biogeosciences Discuss., 5(4), 2839–2865, doi:10.5194/bgd-5-2839-2008, 2008.

Sakamoto, C. M., Johnson, K. S. and Coletti, L. J.: Improved algorithm for the computation of nitrate concentrations in seawater using an in situ ultraviolet spectrophotometer, Limnol. Oceanogr. Methods, 7(1), 132–143, doi:10.4319/lom.2009.7.132, 2009.

Sathyendranath, S. ., Grant, M. ., Brewin, R. J. W. ., Brockmann, C. ., Brotas, V. ., Chuprin, A. ., Doerffer, R. ., Dowell, M. ., Farman, A. ., Groom, S. ., Jackson, T. ., Krasemann, H. ., Lavender, S. ., Martinez Vicente, V.; Mazeran, C. ., Mélin, F. ., Moore, T. S. ., Müller, D. . and Platt, G.: ESA Ocean Colour Climate Change Initiative (Ocean_Colour_cci): Version 3.1 Data., 2018.

Sauzède, R., Lavigne, H., Claustre, H., Uitz, J., Schmechtig, C., D'Ortenzio, F., Guinet, C. and Pesant, S.: Vertical distribution of chlorophyll a concentration and phytoplankton community composition from in situ fluorescence profiles: A first database for the global ocean, Earth Syst. Sci. Data, 7(2), doi:10.5194/essd-7-261-2015, 2015.

Sauzède, R., Claustre, H., Uitz, J., Jamet, C., Dall'Olmo, G., D'Ortenzio, F., Gentili, B., Poteau, A. and Schmechtig, C.: A neural network-based method for merging ocean color and Argo data to extend surface bio-optical properties to depth: Retrieval of the particulate backscattering coefficient, J. Geophys. Res. Ocean., 121(4), 2552–2571, doi:10.1002/2015JC011408, 2016.

Sauzède, R., Bittig, H. C., Claustre, H., Pasqueron de Fommervault, O., Gattuso, J.-P., Legendre, L. and Johnson, K. S.: Estimates of Water-Column Nutrient Concentrations and Carbonate System Parameters in the Global Ocean: A Novel Approach Based on Neural Networks, Front. Mar. Sci., 4, 128, doi:10.3389/fmars.2017.00128, 2017.

Schmechtig, C., Claustre, H., Poteau, A. and D'Ortenzio, F.: Bio-Argo quality control manual for the Chlorophyll-A concentration, Argo data management., 2014.

Schmechtig, C., Poteau, A., Claustre, H., D'Ortenzio, F., Dall'Olmo, G. and Boss, E.: Processing Bio-Argo particle backscattering at the DAC level, Argo data management., 2016.

Signorini, S. R., McClain, C. R. and Dandonneau, Y.: Mixing and phytoplankton bloom in the wake of the Marquesas Islands, Geophys. Res. Lett., 26(20), 3121–3124, doi:10.1029/1999GL010470, 1999.

Stramska, M., Stramski, D., Hapter, R., Kaczmarek, S. and Stoń, J.: Bio-optical relationships and ocean color algorithms for the north polar region of the Atlantic, J. Geophys. Res., 108(C5), 3143, doi:10.1029/2001JC001195, 2003.

Stramski, D., Reynolds, R. A., Kahru, M. and Mitchell, B. G.: Estimation of Particulate Organic Carbon in the Ocean from Satellite Remote Sensing, Science, 285(5425), 239–242, doi:10.1126/science.285.5425.239, 1999.

Stramski, D., Reynolds, R. A., Babin, M., Kaczmarek, S., Lewis, M. R., Röttgers, R., Sciandra, A., Stramska, M., Twardowski, M. S., Franz, B. A. and Claustre, H.: Relationships between the surface concentration of particulate organic carbon and optical properties in the eastern South Pacific and eastern Atlantic Oceans, Biogeosciences, 5(1), 171–201, doi:10.5194/bg-5-171-2008, 2008.

Suga, T., Motoki, K., Aoki, Y., Macdonald, A. M., Suga, T., Motoki, K., Aoki, Y. and Macdonald, A. M.: The North Pacific Climatology of Winter Mixed Layer and Mode Waters, J. Phys. Oceanogr., 34(1), 3–22, doi:10.1175/1520-0485(2004)034<0003:TNPCOW>2.0.CO;2, 2004.

Thierry, V., Gilbert, D., Kobayashi, T., Schmid, C. and Kanako, S.: Processing Argo oxygen data at the DAC level cookbook, Argo data management., 2016.

Toyoda, T., Fujii, Y., Kuragano, T., Kamachi, M., Ishikawa, Y., Masuda, S., Sato, K., Awaji, T., Hernandez, F., Ferry, N., Guinehut, S., Martin, M. J., Peterson, K. A., Good, S. A., Valdivieso, M., Haines, K., Storto, A., Masina, S., Köhl, A., Zuo, H., Balmaseda, M., Yin, Y., Shi, L., Alves, O., Smith, G., Chang, Y.-S., Vernieres, G., Wang, X., Forget, G., Heimbach, P., Wang, O., Fukumori, I. and Lee, T.: Intercomparison and validation of the mixed layer depth fields of global ocean syntheses, Clim. Dyn., 1–21, doi:10.1007/s00382-015-2637-7, 2015.

Wagener, T., Guieu, C., Losno, R., Bonnet, S. and Mahowald, N.: Revisiting atmospheric dust export to the Southern Hemisphere ocean: Biogeochemical implications, Global Biogeochem. Cycles, 22(2), GB2006, doi:10.1029/2007GB002984, 2008.

Williams, G. J., Gove, J. M., Eynaud, Y., Zgliczynski, B. J. and Sandin, S. A.: Local human impacts decouple natural biophysical relationships on Pacific coral reefs, Ecography (Cop.)., 38(8), 751–761, doi:10.1111/ecog.01353, 2015.

Winn, C. D., Campbell, L., Christian, J. R., Letelier, R. M., Hebel, D. V., Dore, J. E., Fujieki, L. and Karl, D. M.: Seasonal variability in the phytoplankton community of the North Pacific Subtropical Gyre, Global Biogeochem. Cycles, 9(4), 605–620, doi:10.1029/95GB02149, 1995.

Wong, A., Keely, R., Carval, T. and Argo Data Management Team: Argo Quality Control Manual for CTD and Trajectory Data, Argo data management., 2015.

Xing, X., Claustre, H., Blain, S., D'Ortenzio, F., Antoine, D., Ras, J. and Guinet, C.: Quenching correction for in vivo chlorophyll fluorescence acquired by autonomous platforms: a case study with instrumented elephant seals in the Kerguelen region (Southern Ocean), Limnol. Oceanogr. Methods, 10, 483–495, doi:10.4319/lom.2012.10.483, 2012.
Xing, X., Claustre, H., Boss, E., Roesler, C., Organelli, E., Poteau, A., Barbieux, M. and D'Ortenzio, F.: Correction of profiles of in-situ chlorophyll fluorometry for the contribution of fluorescence originating from non-algal matter, Limnol. Oceanogr. Methods, 15(1), 80–93, doi:10.1002/lom3.10144, 2017.

Zhang, W.-Z., Wang, H., Chai, F. and Qiu, G.: Physical drivers of chlorophyll variability in the open South China Sea, J. Geophys. Res. Ocean., 121(9), 7123–7140, doi:10.1002/2016JC011983, 2016.

Table 1. Summary of the mission and equipment relative to each BGC-Argo float used in this study.

Float	WMO #	Length of the mission	UTC date of deployment (dd/mm/YYYY)	Position of deployment (lon/lat)	UTC date of last profile (dd/mm/YYYY)	Temporal and vertical resolution of data acquisition	Equipment
FOpenO	6901687	19 months	03/04/2015	-149.7/-18.24	25/11/2016	Temporal resolution: -daily from 03/04/2015 to 16/07/2015 -5 days from 16/07/2015 to 25/11/2016 Vertical resolution: -every m from the surface to 250 m -every 10 m from 250 m to 1000 m	-CTD -Radiometry -WET Labs ECO Puck Triplet
FLeeT	6901659	~3 months	15/10/2015	-149.1/-18.20	10/01/2016	Temporal resolution: Daily Vertical resolution: -every m from the surface to 350 m -every 10 m from 350 m to 1000 m	-CTD -Radiometry -WET Labs ECO Puck Triplet -Nitrate sensor (SUNA) -Oxygen sensor (Aanderaa optode)

Table 2. Symbols of variables used in this study with their definitions and units.

Symbol	Definition	Units
PAR	Photosynthetically Available Radiation	mol photons m^{-2} day^{-1}
Chl	Chlorophyll *a* concentration	mg m^{-3}
b_{bp}	Particulate backscattering coefficient at 700 nm	m^{-1}
POC	Particulate Organic Carbon	mg m^{-3}
b_{bp}/Chl	Ratio of b_{bp} to Chl	m^2 mg^{-1}
O_2	Oxygen concentration	µmol kg^{-1}
NO_3^-	Nitrate concentration	µmol kg^{-1}
MLD	Mixed Layer Depth	m
σ	Potential Density computed from Temperature and Salinity	kg m^{-3}
PAR_{ML}	Average value of PAR in the mixed layer	mol photons m^{-2} day^{-1}
Chl_{surf}	Mean of Chl in the first penetration layer (from surface to Z_{pd} depth)	mg m^{-3}
b_{bp_surf}	Mean of b_{bp} in the first penetration layer (from surface to Z_{pd} depth)	m^{-1}
b_{bp_surf}/Chl_{surf}	Mean of b_{bp}/Chl in the first penetration layer (from surface to Z_{pd} depth)	m^2 mg^{-1}
Z_{pd}	First penetration depth	m
K_d(PAR)	diffuse attenuation coefficient	m^{-1}
PAR(0^-)	PAR just below the surface	mol photons m^{-2} day^{-1}
Z_{eu}	Euphotic depth	m
FSLE	Finite Size Lyapunov Exponents	d^{-1}
T	Conservative Temperature	°C
S	Absolute Salinity	g kg^{-1}

Table 3. Number of profiles, mean and range values in brackets of monthly-mean DCM depth (m), DCM value (mg m^{-3}), MLD (m), Chl_{surf} (mg m^{-3}) and POC_{Surf} (mg m^{-3}) for FOpenO float.

Parameter	Jan.	Feb.	Mar.	Apr.	May	Jun.	Jul.	Aug.	Sept.	Oct.	Nov.	Dec.
N_{obs}	6	6	6	37	36	36	25	12	12	13	11	6
DCM depth (min – max)	131 (123 – 140)	135 (128 – 147)	137 (130 – 147)	118 (98 – 132)	124 (104-147)	107 (89-133)	112 (95-134)	115 (95-138)	140 (101-177)	135 (115-161)	138 (107-160)	136 (112-153)
DCM value (min – max)	0.35 (0.29 – 0.38)	0.31 (0.22 – 0.40)	0.30 (0.25 – 0.33)	0.26 (0.19 – 0.37)	0.24 (0.17-0.34)	0.24 (0.20-0.28)	0.26 (0.23-0.31)	0.29 (0.25-0.38)	0.27 (0.21-0.35)	0.29 (0.22-0.38)	0.30 (0.23-0.42)	0.32 (0.23-0.41)
MLD (min – max)	45 (31 – 53)	31 (10 – 51)	49 (34 – 63)	46 (10 – 70)	62 (34-87)	79 (49-113)	84 (46-115)	72 (24-109)	68 (31-103)	57 (10-116)	38 (10-62)	42 (32-61)
Chl_{surf} (min – max)	0.01 (0.01 – 0.02)	0.01 (0.01 – 0.01)	0.01 (0.01 – 0.02)	0.02 (0.01 – 0.04)	0.04 (0.01-0.07)	0.05 (0.01-0.08)	0.04 (0.01-0.06)	0.02 (0.01-0.06)	0.01 (0-0.04)	0.02 (0-0.04)	0.01 (0.01-0.03)	0.01 (0-0.02)
POC_{Surf} (min – max)	31 (30 – 32)	31 (30 – 32)	32 (30 – 35)	37 (28 – 46)	39 (30 – 50)	40 (30 – 50)	34 (30 – 41)	35 (32 - 41)	32 (31 – 35)	32 (30 – 34)	33 (29 – 38)	34 (32 – 36)

Table 4. Number of profiles, mean and range values in brackets of monthly-mean DCM depth (m), DCM value (mg m^{-3}), MLD (m), Chl_{surf} (mg m^{-3}) and POC_{Surf} (mg m^{-3}) for FLeeT float

Parameter	Oct.	Nov.	Dec.	Jan.
Nobs	17	30	31	10
DCM depth (min – max)	128 (113 – 150)	124 (98 – 156)	135 (90 – 157)	146 (116 - 169)
DCM value (min – max)	0.3 (0.23 – 0.35)	0.35 (0.24 – 0.44)	0.24 (0.17 – 0.30)	0.25 (0.19 – 0.31)
MLD (min – max)	98 (28 – 127)	40 (10 – 65)	34 (10 – 61)	35 (24 – 42)
Chl_{surf} (min – max)	0.04 (0.01 – 0.1)	0.02 (0.01 – 0.05)	0.02 (0.01 – 0.05)	0.02 (0.01 – 0.03)
POC_{Surf} (min – max)	35 (33 - 39)	37 (33 – 39)	45 (28 – 141)	32 (29 – 36)

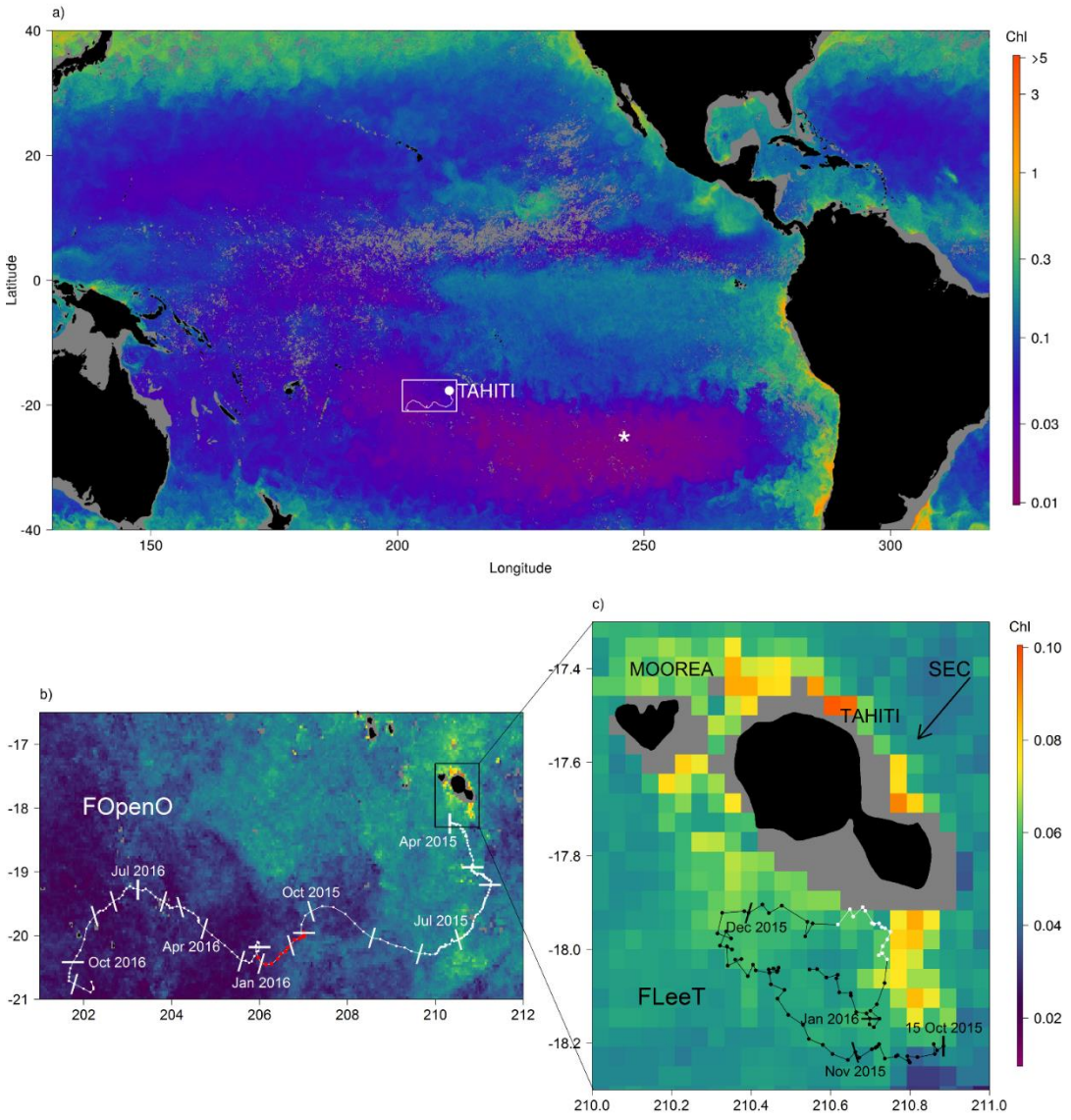

Figure 1: (a) Spatial distribution of OC-CCI surface satellite Chl (mg m^{-3}) in December 2015 for the Pacific Ocean. Our study area and the island of Tahiti are represented by the white rectangle and the white point respectively. The white star represents the geographic area of the M2014 reference study (see Section 3.1). The trajectories of (b) FOpenO float and (c) FLeeT float are shown with background color representing the OC-CCI surface satellite Chl (mg m^{-3}) distribution in December 2015. In panel b FOpenO profiles concomitant with FLeeT profiles acquisition are coloured in red. In panel c the period two from FLeeT is coloured in white (see Section 3.3.1). Grey pixels represent missing data because of clouds or the 500 m bathymetric mask that removed nearshore pixels that could be biased by land and the surrounding lagoon. Islands and continents are indicated in black. The islands of Moorea and Tahiti are indicated and the mean direction of the South Equatorial Current (SEC) is indicated by the arrow in panel c.

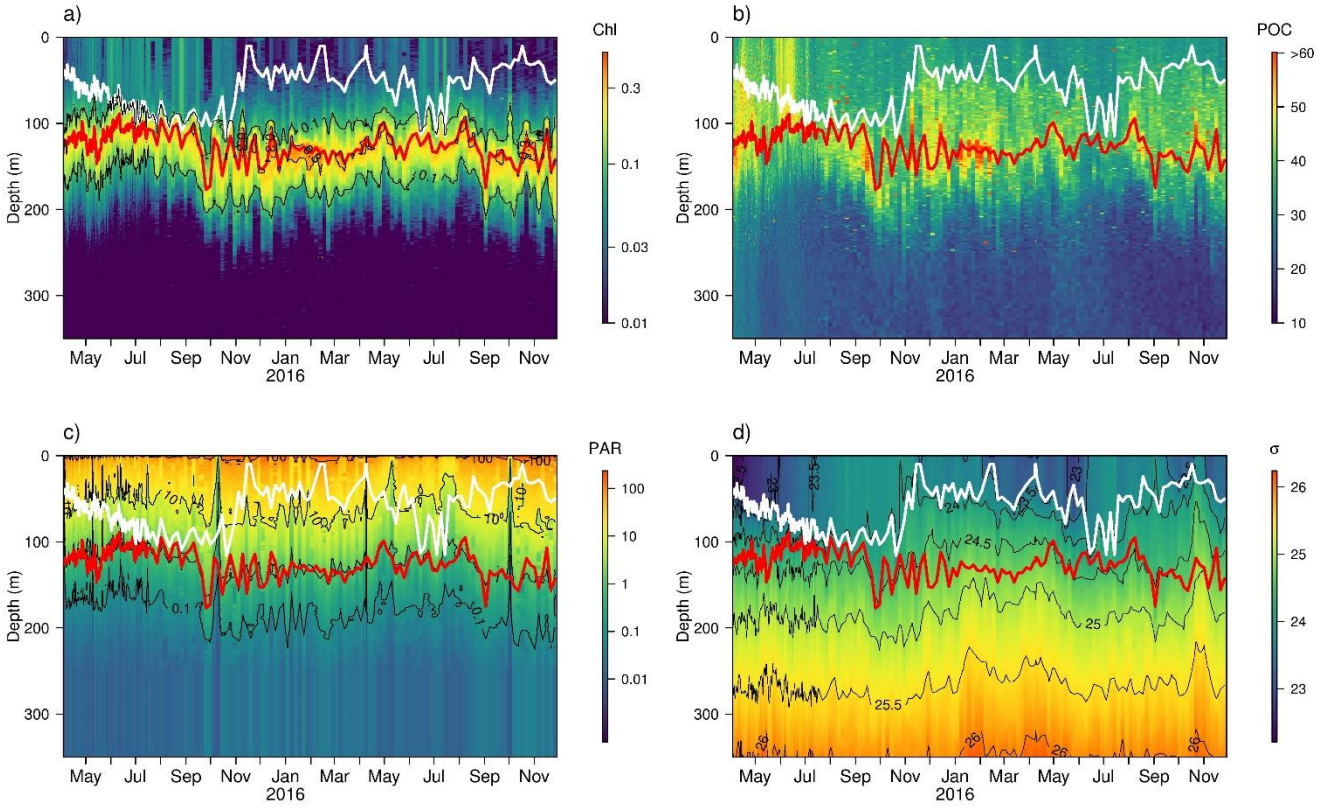

Figure 2: FOpenO vertical distribution against time of (a) Chl (mg m^{-3}) with the 0.1, 0.2 and 0.3 mg m^{-3} isocontours as dotted black lines, (b) POC (mg m^{-3}), (c) PAR (mol photons m^{-2} d^{-1}) with the 0.1, 1 and 10 mol photons m^{-2} d^{-1} isolumes as dotted black lines and (d) density (kg m^{-3}) with isopycnes (interval = 0.5 kg m^{-3}, dotted black lines). In each panel, the white and red lines show the MLD and the depth of the DCM, respectively. The black vertical solid lines represent the second period of acquisition from FLeeT (see Section 3.3.1).

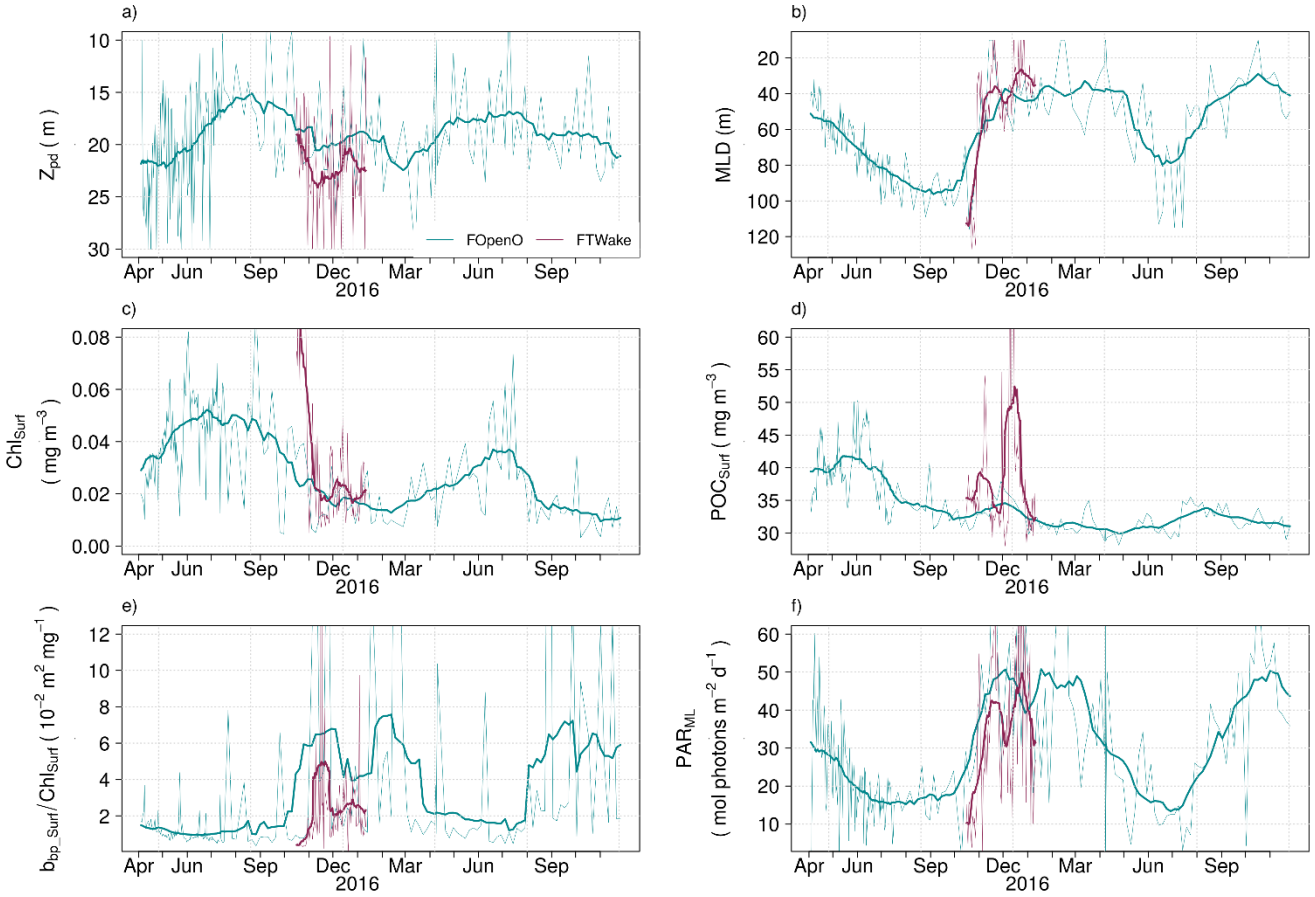

Figure 3: **Time series of the mean-filtered FOpenO (±30 days, blue line) and FLeeT (± 10 days, purple line) observations represented as bold lines and high frequency observations represented as thin lines of the (a) first penetration depth (Z_{pd}, m), (b) mixed layer depth (MLD, m), (c) 0- Z_{pd} integrated Chl (Chl_{surf}, mg m^{-3}), (d) 0- Z_{pd} integrated POC (POC_{Surf}, m^{-1}), (e) 0- Z_{pd} integrated ratio of b_{bp} to Chl (b_{bp_surf}/Chl_{surf}, m^2 mg^{-1}), and (f) average PAR in the mixed layer (PAR_{ML}, mol photons m^{-2} d^{-1}).**

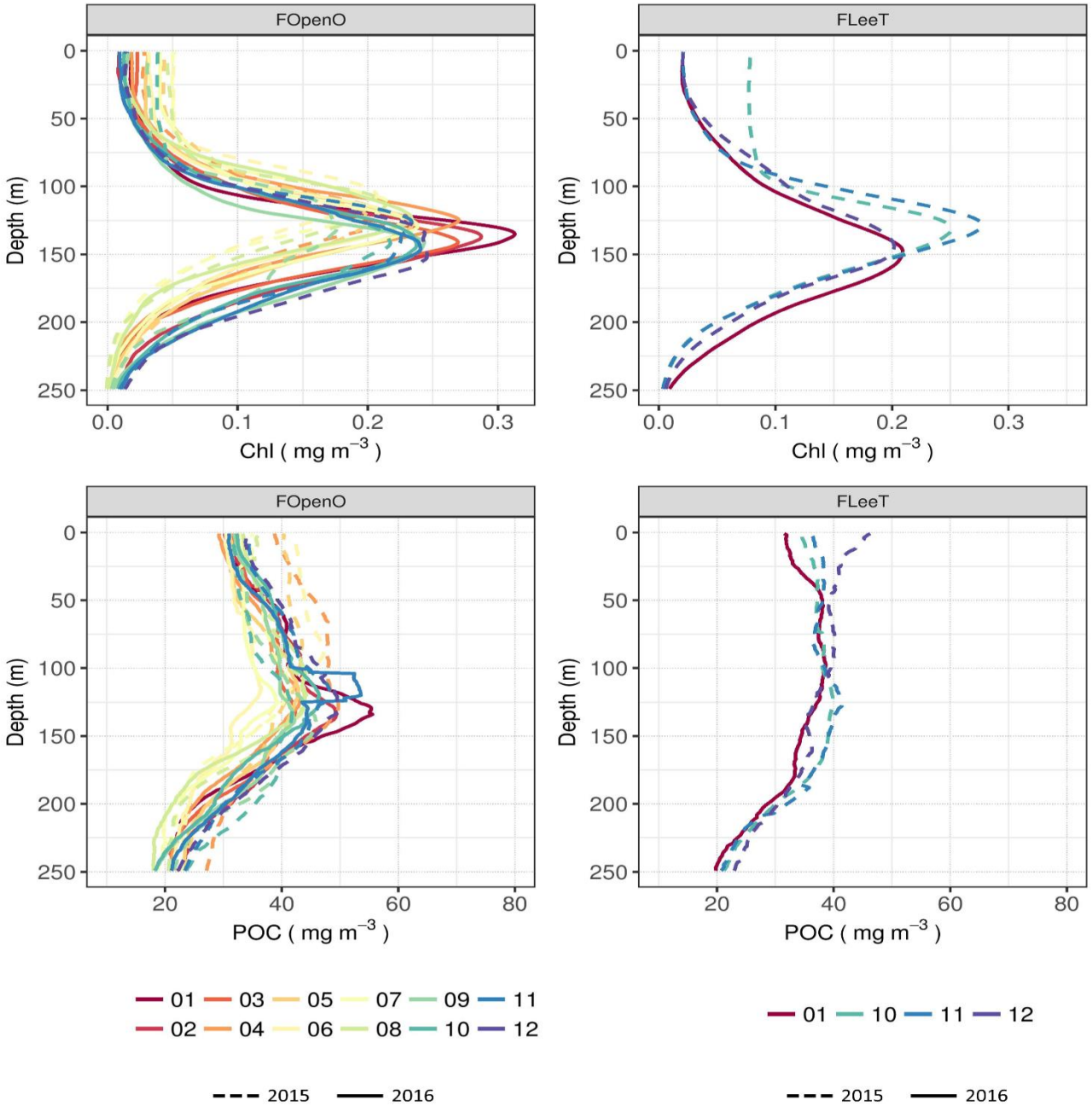

Figure 4: **Vertical distribution of monthly average Chl (mg m^{-3}; upper panels) and POC (mg m^{-3}; lower panels), for the FOpenO float (left) and FLeeT float (right). The color code represents the months from January to December.**

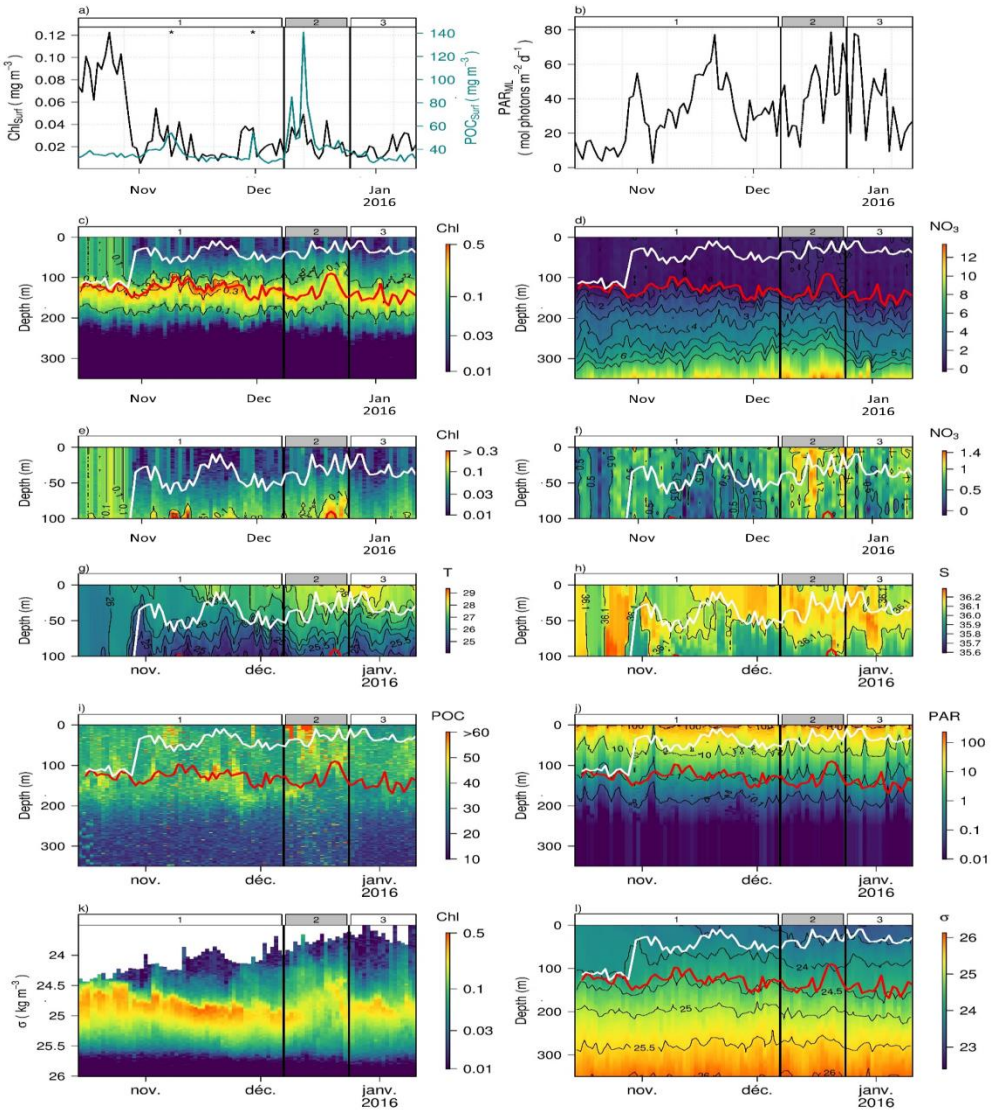

Figure 5: **Biogeochemical parameters measured from FLeeT. Vertical distribution along time of (a) Chl_{surf} (left axis, black) and POC_{Surf} (right axis, blue) and (b) PAR_{ML}. These time-series represent the unfiltered time series of Figures 3c, d and f, respectively. The black stars in panel (a) are defined in Section 3.3.1. Vertical distribution against time of: (c) Chl (mg.m^{-3}) with the 0.1 and 0.3 mg.m^{-3} isocontours as black lines, (d) nitrate concentration (µmol kg^{-1}) with isonitrates (µmol kg^{-1}, black lines with interval=1 µmol kg^{-1}). (e) and (f) panels represent the 0 - 100 m zoom of (c) and (d) panels. (g) and (h) panels represent the 0-100 m vertical distribution of T (°C) and S with isocontours as black lines. Time series of (i) POC (mg m^{-3}) and (j) PAR (mol photons m^{-2} d^{-1}) with isolumes (0.1, 1 and 10 mol photons m^{-2} d^{-1}, black lines). (k) Time series of Chl (mg.m^{-3}) as a function of density (kg m^{-3}). (l) Vertical distribution of density (kg m^{-3}) against time with isopycnes (kg m^{-3}, black lines with interval=0.5 kg m^{-3}). The white and red lines represent the MLD and the location of the DCM depth, respectively. The black vertical solid lines in each panel indicate three specific time periods as defined in Section 3.3.1.**

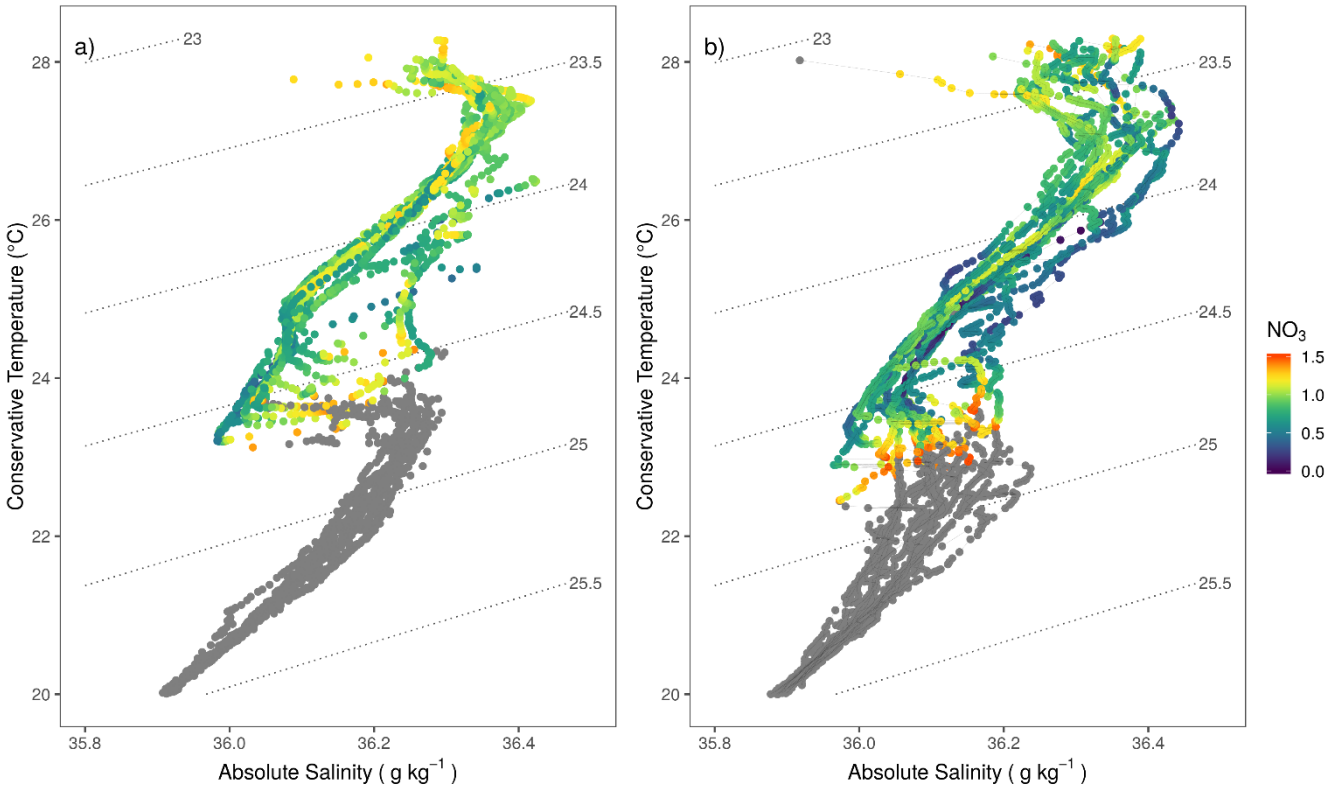

Figure 6: TS diagrams issued from FLeeT during (a) period 2 and (b) period 3 as defined in Section 3.3.1. Black dotted lines represent isopycnal surfaces (interval= 0.5 kg m^{-3}). Colours refer to NO_3^- concentrations (µmol kg^{-1}). NO_3^- higher than 1.5 µmol kg^{-1} are in grey.

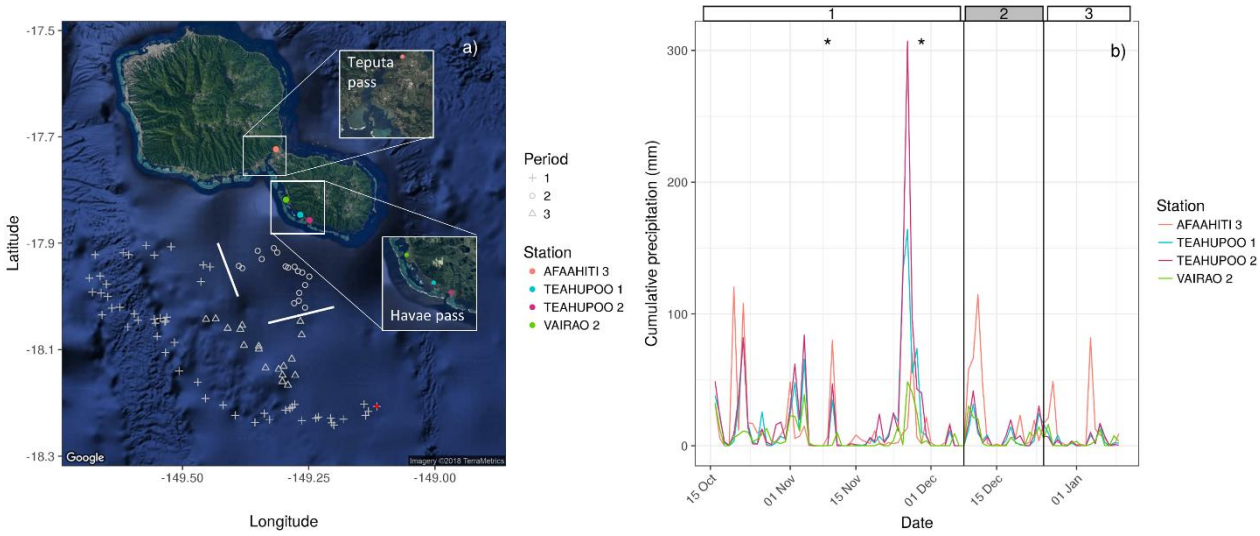

Figure 7: **Meteorological data during FLeeT lifetime. (a) The FLeeT trajectory is plotted as grey points. The red point indicates the location of the float deployment. Different time periods, as defined in Section 3.3.1, are delimited by the white bars along the trajectory of the float. The locations of the 4 Météo-France meteorological stations are detailed in the different insets. (b) Time series of daily cumulative precipitation measured at the 4 stations localized on panel (a). The two black stars refer to the two POC maxima observed during the first period, identified in Figure 5a and discussed in Section 3.3.2. The black vertical solid lines indicate three specific time periods as defined in Section 3.3.1.**

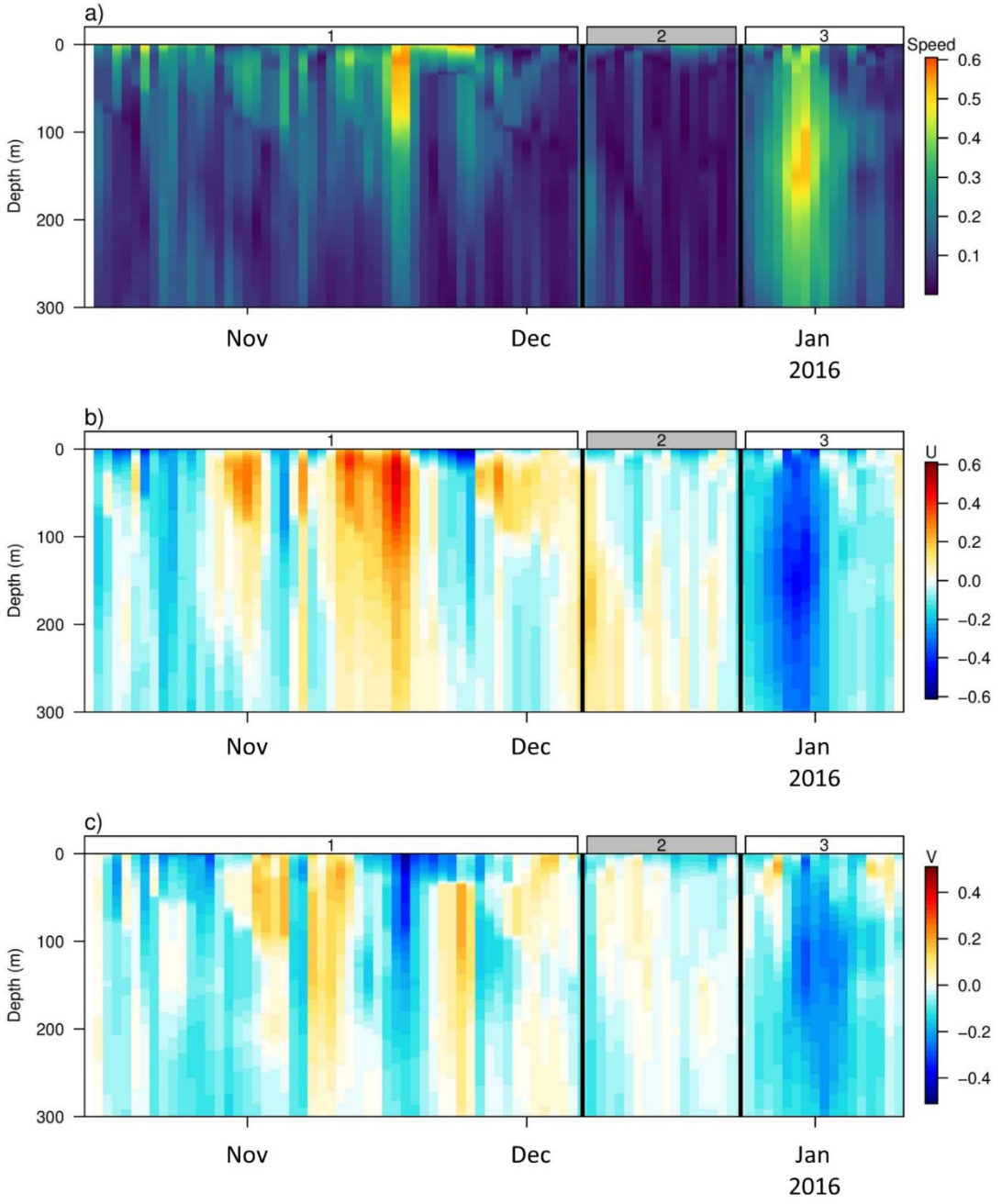

Figure 8: **Time series of the 0 - 300 m HYCOM-modelled current along the FLeeT track: (a) current amplitude (speed, m s^{-1}), (b) zonal (U, m s^{-1}) and (c) meridian components (V, m s^{-1}). In panel (b) negative values represent westward currents while positive values represent eastward currents. In panel (c), negative values represent southward currents while positive values represent northward currents. The black vertical solid lines in each panel indicate three specific time periods as defined in Section 3.3.1.**

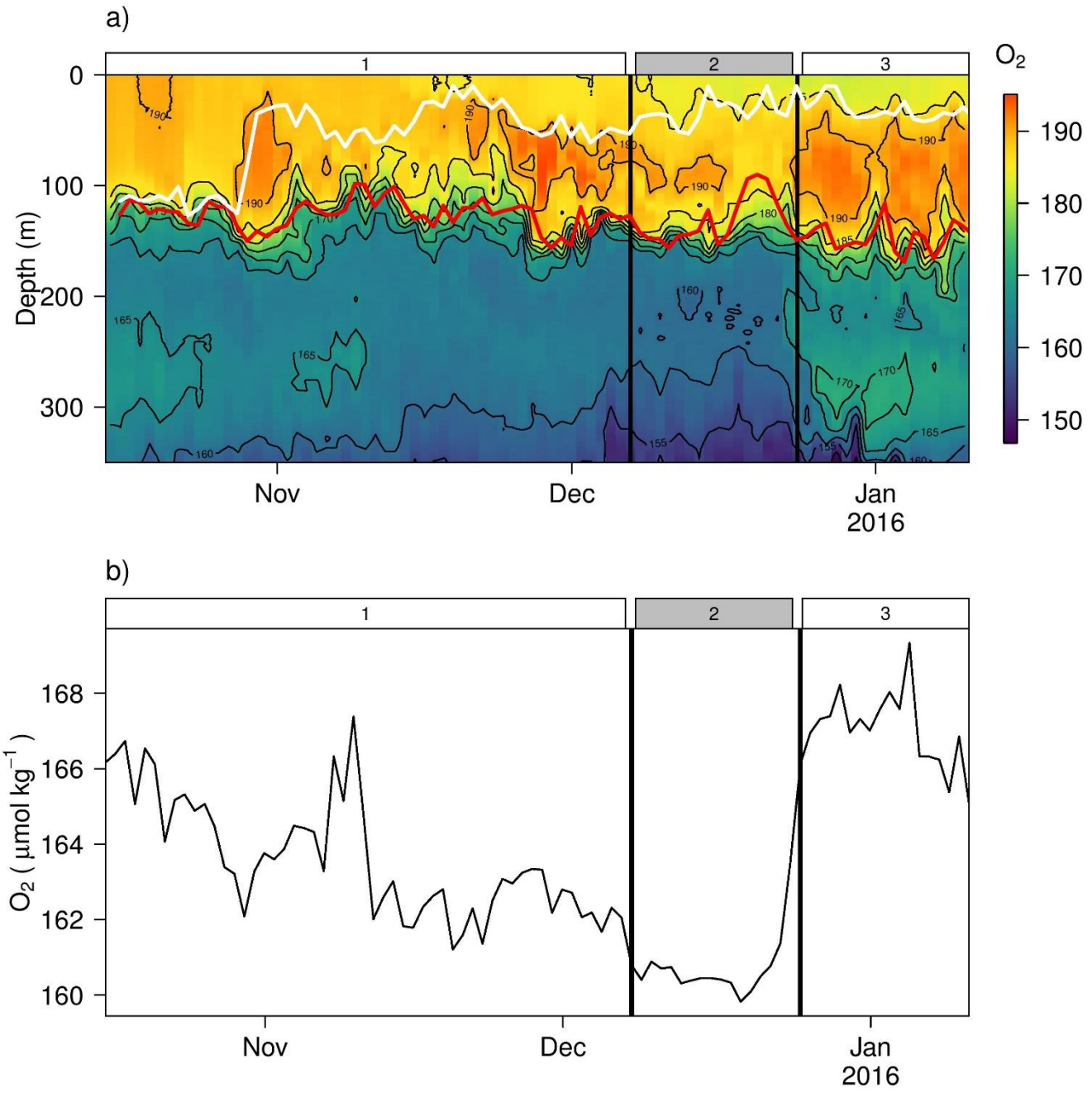

Figure 9: **(a) vertical distribution of FLeeT O_2 (µmol kg^{-1}) along time. Isolines are indicated as black lines (interval=5 µmol kg^{-1}). The white and red lines represent the MLD and the location of the DCM depth, respectively. (b) FLeeT O_2 averaged over 300 m ± 10 m. The black vertical solid lines in each panel indicate three specific time periods as defined in Section 3.3.1.**

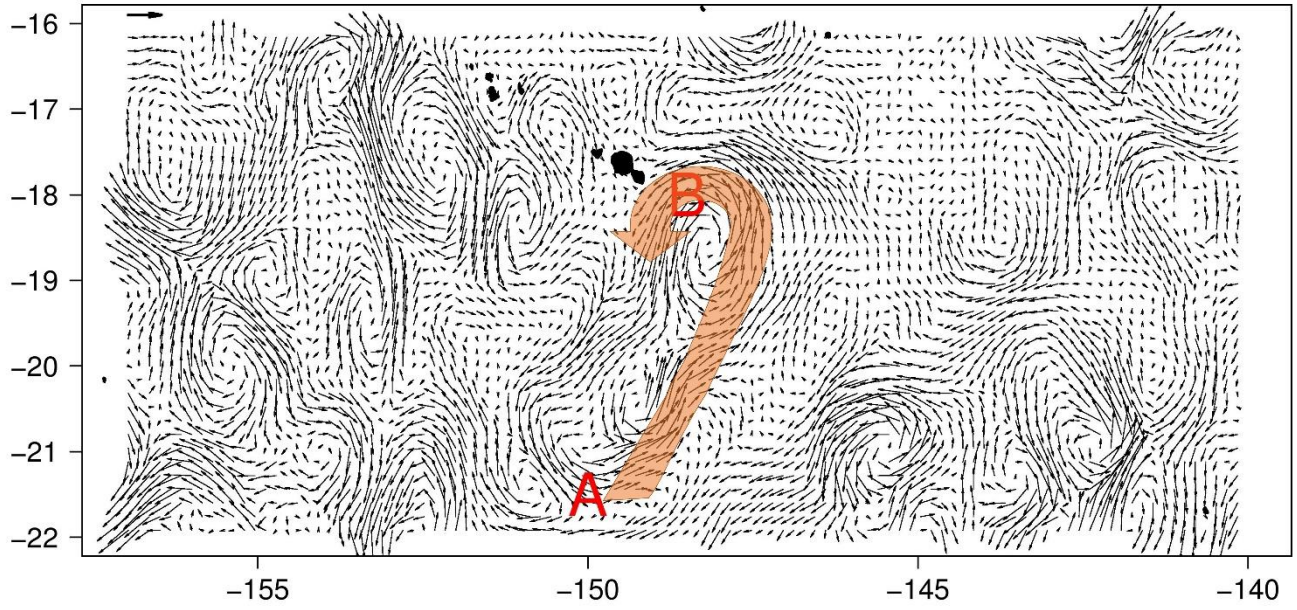

Figure 10: HYCOM modelled current (m s^{-1}) at 300 m depth for 04/12/2015, 24 days before the incursion of the more oxygenated waters measured from FLeeT. The reference arrow (in bold) is in the top left of the panel and represents 0.5 m s^{-1}. The arrow and the points A and B are defined in Section 3.3.2.

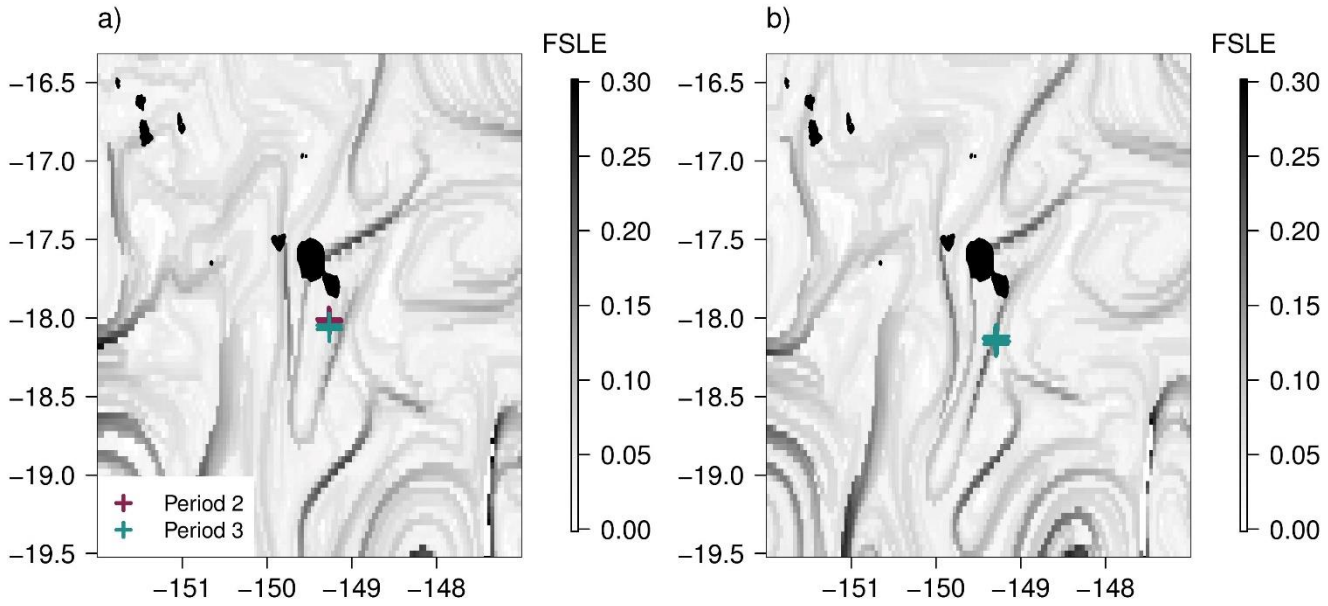

Figure 11: Spatial distribution of Finite Size Lyapunov Exponents (FSLEs, d^{-1}) represented by the grey color bar for the four days around (a) 24/12/2015 and (b) 28/12/2015. Crosses in panels (a) and (b) represent the FLeeT position with colors referring to the corresponding periods. For each map, several crosses are plotted since FSLEs are plotted for four days while FLeeT has a one day temporal resolution of data acquisition.

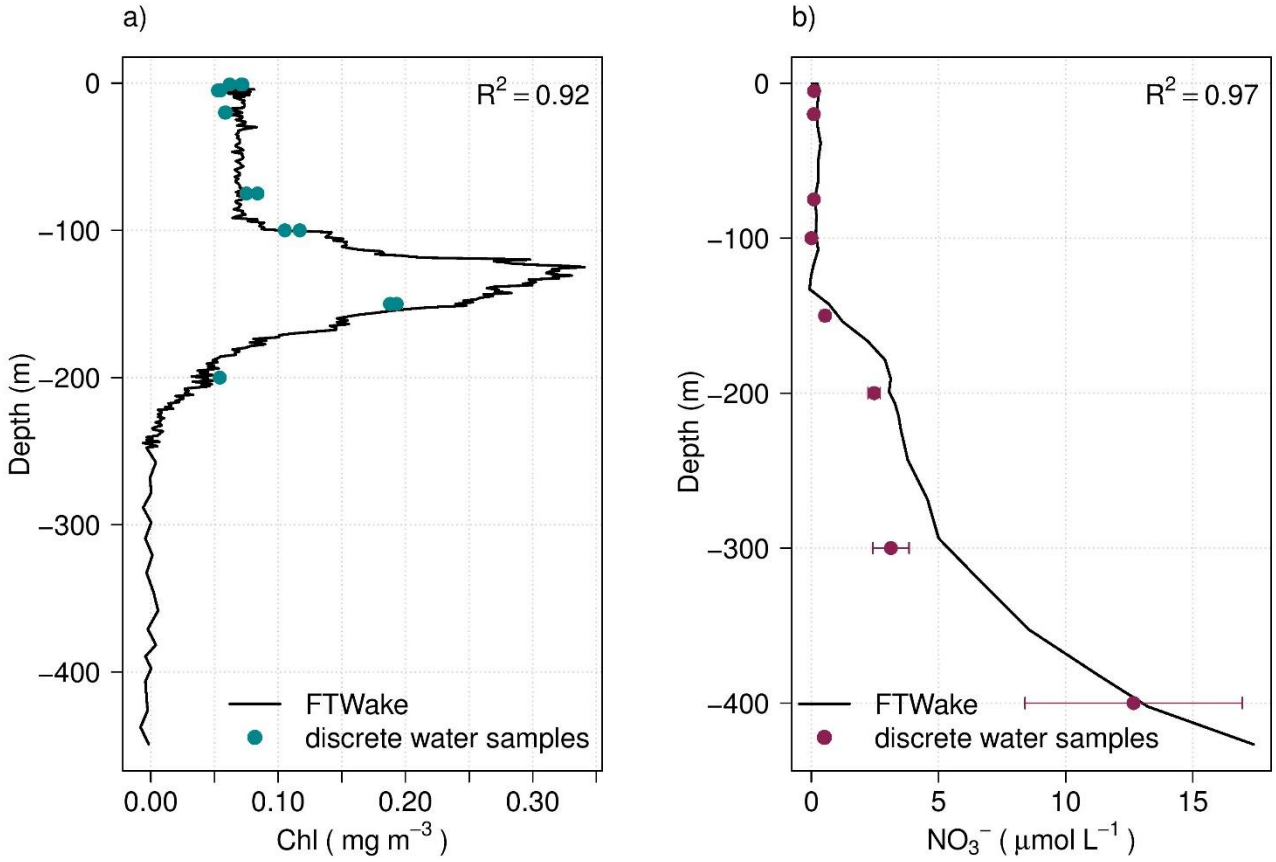

Figure S1 Comparisons at FLeeT deployment of (a) HPLC-based Chl concentration (blue points) with the concomitant float Chl profile (continuous black line) and (b) *in situ* NO_3^- estimates (from laboratory analyses; purple points with the error bar representing the standard deviation) and concomitant NO_3^- profile (continuous black line). No error bars are plotted for HPLC-based Chl estimations in panel (a) because two values maximum are available for each depth.

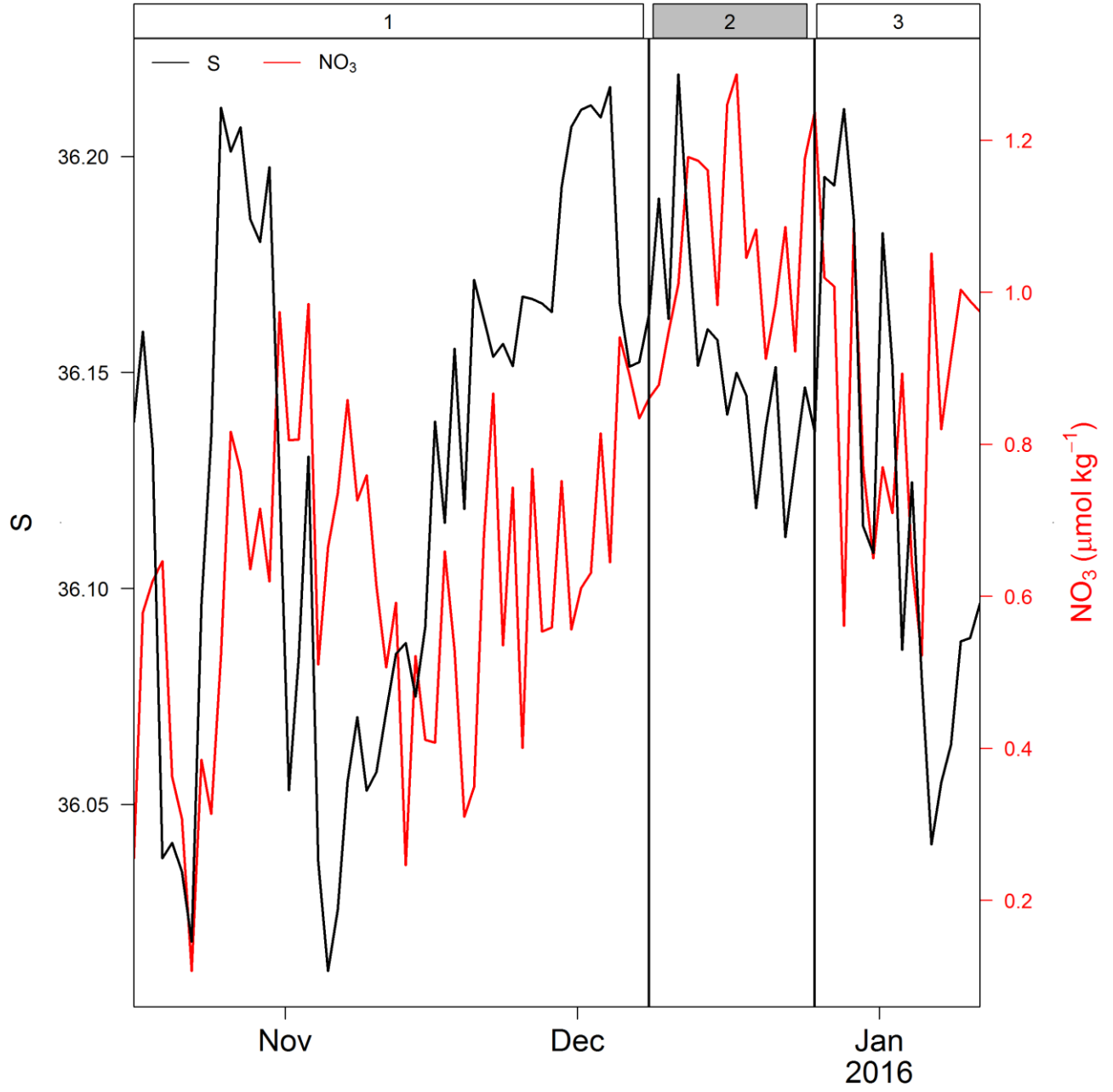

Figure S2: Surface salinity (left axis, black) and nitrate concentration (right axis, red) measured from FLeeT float. The black vertical solid lines in each panel indicate three specific time periods as defined in Section 3.3.1.

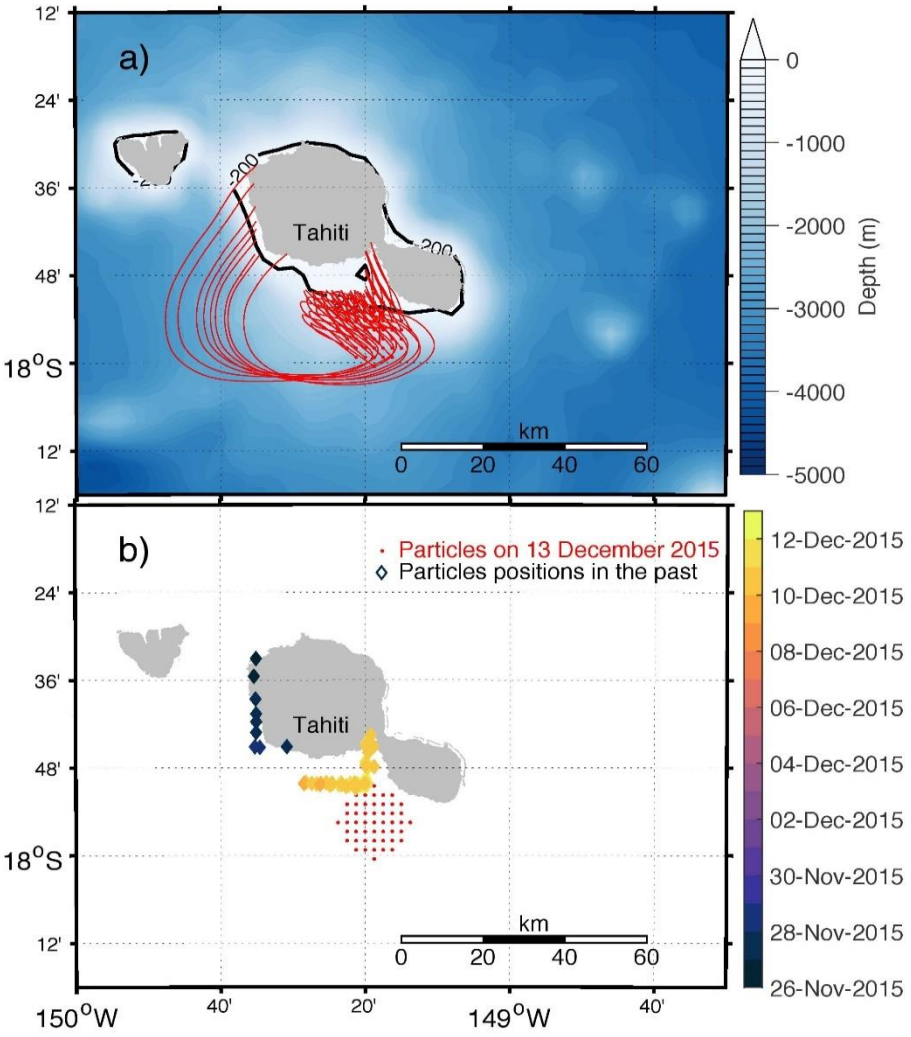

Figure S3: Backward tracking of Lagrangian particles with (a) the trajectories in red lines and (b) the original position (red dots) and dates of particles when they "touch" the coast (coloured diamonds). Note however that the HYCOM model does not resolve the Tahitian coast in high resolution.

Highlights

- A biological enhancement is observed leeward Tahiti from a Biogeochemical-Argo float
- Observed nitrate increase in the upper-lit layer likely results from land drainage
- Phytoplankton community composition leeward Tahiti probably differs from open ocean
- The open ocean summer deepening of the deep chlorophyll maximum is light-driven
- The wintertime increase in surface chlorophyll results from photoacclimation